

34. PALEOMAGNETIC INVESTIGATIONS OF VOLCANIC ROCKS: PALEOLATITUDES OF THE NORTHWESTERN PACIFIC GUYOTS¹

Masao Nakanishi² and Jeffrey S. Gee³

ABSTRACT

Paleomagnetic properties of 340 minicore samples from 5 guyots in the northwestern Pacific Ocean were measured on board the *JOIDES Resolution* and in the paleomagnetic laboratories of the Ocean Research Institute, University of Tokyo, and of Lamont-Doherty Earth Observatory. Stepwise thermal and alternating-field (AF) demagnetizations typically isolate the same characteristic magnetization direction. The shipboard and shore-based paleomagnetic measurements suggest a paleolatitude of ~10°S for Limalok, Wodejebato, MIT, and Takuyo-Daisan guyots. Lo-En Guyot apparently was constructed at a latitude of 31°S. According to the radiometric age of volcanic rocks from MIT Guyot, the reversed polarity of the volcanic basement of MIT Guyot corresponds to Chron M1 or older. A reversed polarity remanence of Wodejebato Guyot was acquired during Chron C33R because radiometric age determinations for Wodejebato Guyot range from 79 to 85 Ma. Our paleolatitude estimates for Lo-En, MIT, and Takuyo-Daisan guyots differ from those derived from previous seamount magnetic anomaly modeling. The sense and magnitude of this paleolatitude discrepancy are consistent with a significant contribution from viscous and induced magnetizations. We estimated the paleolatitudes of the guyots from the age data and from a previously published absolute-motion model for the Pacific Plate. Differences between these paleolatitude estimates and those derived from paleomagnetic measurements except for Wodejebato Guyot are smaller than 6°.

INTRODUCTION

There are many seamounts and guyots in the western Pacific Ocean. Flat-topped seamounts in the western Pacific Ocean were first described in the 1940s by H.H. Hess (1946) and were named "guyots" after the 19th-century geographer, Arnold Guyot. Most of the seamounts and guyots in the western Pacific Ocean lie on crust of Mesozoic (Late Jurassic to mid-Cretaceous) age and formed during the Cretaceous. Previous studies (e.g., Duncan and Clague, 1985) suggest that most of these seamounts were constructed in the Southern Hemisphere, in a region presently characterized by abundant hotspot volcanism. This region, known as the South Pacific Superswell (McNutt and Fischer, 1987), may have been active since the Cretaceous (e.g., Larson, 1991; Fukao, 1992). An understanding of past superswell activity, as manifest by seamounts and guyots in the western Pacific Ocean, is necessary for unravelling the evolution and past motions of the Pacific Plate.

Ocean Drilling Program (ODP) Leg 144 drilled five guyots in the western Pacific Ocean (Table 1; see site map preceding title page). With one exception (Site 880), volcanic material was recovered at each site, providing information on the paleolatitudes of these guyots. The results of shipboard measurements are described in detail in the Leg 144 *Initial Reports* volume (Premoli Silva, Haggerty, Rack, et al., 1993). Shipboard paleomagnetic studies suggest that these guyots were all formed in the Southern Hemisphere. Shore-based paleomagnetic studies of discrete volcanic samples have focused on refining the paleolatitude estimates and on evaluating the nature of the remanence. This article describes the results of paleomagnetic studies that combined both on-board and shore-based measurements. The Fe-Ti oxide mineralogy and rock magnetic properties of volcanic rocks used in this study are described in Gee and Nakanishi (this volume).

METHOD OF PALEOMAGNETIC MEASUREMENTS

Paleomagnetic measurements were conducted on 340 minicore samples, both on board the *JOIDES Resolution* and in the paleomagnetic laboratories of the Ocean Research Institute (ORI), University of Tokyo, and of Lamont-Doherty Earth Observatory (LDEO). Sampling locations and other data are summarized in Table 2. To obtain the most reliable paleomagnetic directions, all samples were subjected to either stepwise alternating-field (AF) or thermal demagnetization. Whole-core remanence measurements on the volcanic rocks of Sites 878 and 879 were also made on board with a 2-G Enterprises (Model 760R) pass-through cryogenic magnetometer. The sampling interval of the whole-core measurements was 5 cm. Shipboard remanence measurements of discrete samples were also made with the cryogenic magnetometer following AF demagnetization with a Schonstedt geophysical specimen demagnetizer (Model GSD-1; see "Paleomagnetism" section, "Explanatory Notes" chapter, in Premoli Silva, Haggerty, Rack, et al., 1993).

Shore-based paleomagnetic measurements for discrete samples at the ORI were made with a Schonstedt digital spinner magnetometer (Model DSM-2). The AF and thermal demagnetizations in the laboratory were conducted with a Schonstedt geophysical tumbling-specimen demagnetizer (Model GSD-5) and a Schonstedt thermal specimen demagnetizer (Model TSD-1), respectively. Initial susceptibilities of samples were measured by a BISON magnetic susceptibility meter (Model 3101A).

Samples were also measured at Lamont-Doherty Earth Observatory using a 2-G Enterprises cryogenic magnetometer housed in a shielded room. The AF demagnetizations were conducted with a Schonstedt GSD-1, and thermal demagnetizations were done in a large-capacity oven with three separate temperature controllers and an ambient field of smaller than 5 through 8 nT. Susceptibilities of samples at LDEO were determined using a Bartington susceptibility meter.

DATA ANALYSES

Remanence directions after progressive demagnetization were plotted on a Zijderveld diagram (Zijderveld, 1967) to determine the original polarity and to select vector endpoints displaying univectorial decay, preferably, to the origin, by visual inspection. The charac-

¹ Haggerty, J.A., Premoli Silva, I., Rack, F., and McNutt, M.K., *Proc. ODP, Sci. Results*, 144; College Station, TX (Ocean Drilling Program).

² Ocean Research Institute, University of Tokyo, 1-15-1 Minamidai Nakano, Tokyo 164, Japan (present address: Scripps Institution of Oceanography, University of California, San Diego, La Jolla, CA 92093-0212, U.S.A.).

³ Lamont-Doherty Earth Observatory, Palisades, NY 10964, U.S.A. (present address: Scripps Institution of Oceanography, University of California, San Diego, La Jolla, CA 92093-0215, U.S.A.).

Table 1. Site summary, Leg 144.

Hole	Latitude	Longitude	Water depth (m)	Hole depth (mbsf)	Thickness of volcanic rocks (m)
Limalok Guyot:					
871A	5°33.43'N	172°20.66'E	1254.6	151.9	
871B	5°33.44'N	172°20.66'E	1254.0	152.4	
871C	5°33.44'N	172°20.66'E	1224.6	133.7	48.5
Lo-En Guyot:					
872A	10°05.85'N	162°51.96'E	1083.6	144.0	0.3
872B	10°05.81'N	162°52.00'E	1083.6	77.3	57.1
872C	10°05.86'N	162°52.00'E	1083.6	148.0	2.0
Wodejebato Guyot:					
873A	11°53.80'N	164°55.19'E	1334.0	54.3	57.2
873B	11°53.84'N	164°55.23'E	1334.0	69.0	
874A	12°00.22'N	164°56.39'E	1374.9	7.0	
874B	12°00.23'N	164°56.39'E	1374.9	193.5	
875A	12°00.76'N	164°56.47'E	1410.8	11.2	
875B	12°06.16'N	164°56.47'E	1409.8	40.0	
875C	12°00.76'N	164°56.47'E	1408.8	133.0	7.0
876A	12°14.80'N	164°55.91'E	1398.8	154.0	8.5
877A	12°01.15'N	164°55.33'E	1354.8	190.5	4.5
MIT Guyot:					
878A	27°19.14'N	150°53.03'E	1326.2	910.0	204.6 (v)
878B	27°19.14'N	150°53.03'E	1325.8	5.8	186.2 (b)
878C	27°19.14'N	150°53.03'E	1325.8	6.0	
Takuyo-Daisan Guyot:					
879A	34°10.46'N	144°18.56'E	1501.0	226.5	35.5
880A	34°12.53'N	144°18.74'E	1525.0	18.4	

Notes: (v) = volcanic basement from Hole 878A, and (b) = polymictic breccia from Hole 878A.

teristic magnetization direction for each sample was calculated by applying the three-dimensional principal component analysis to the set of vectors thus selected (Kirschvink, 1980).

Mean inclinations (and error estimates) were calculated using the McFadden and Reid (1982) method for azimuthally unoriented data based on flow units identified on board. Although the precise number of flow units may be slightly different from this shipboard estimate, this method provides a reasonable method for identifying cooling units that may plausibly represent independent samplings of the geomagnetic field. Within a flow unit, all sample inclinations were given equal weight. Pairs of samples were often taken in close (5–10 cm) proximity to facilitate comparison of AF and thermal demagnetization behavior. Consequently, the within-flow scatter may be somewhat underestimated. Samples (indicated by asterisks in Tables 3 through 8) were not included in the calculation of flow-unit means if they exhibited particularly noisy demagnetization behavior or were obviously different from the remaining samples within a flow unit. For example, samples from more altered flow-top breccia often had inclinations distinct from the remainder of the flow unit. Mean inclinations for each guyot were determined by simply averaging all flow-unit mean inclinations under the assumption that each represents a distinct sampling of the geomagnetic field. Finally, estimates of directional dispersion for each guyot were used to evaluate whether paleosecular variation (PSV) may have been adequately averaged. Comparison of expected and observed directional dispersion (e.g., McFadden, 1980) provides a necessary, but not sufficient, criterion for evaluating the validity of the paleolatitude estimates for the guyots.

RESULTS OF PROGRESSIVE AF AND THERMAL DEMAGNETIZATIONS AF and Thermal Demagnetizations

Each sample was subjected to progressive AF or thermal demagnetization to isolate the direction of a characteristic magnetization. The maximum angular deviation (MAD) provides a quantitative measurement of the precision with which the best-fit line is determined by principal component analysis (Kirschvink, 1980). Butler (1992) indicated that line fits from principal component analyses that yield a

Table 2. Numbers of samples.

Site	Total	On board		Onshore	
		AF	Thermal	AF	Thermal
871	44	19	8	17	
872	43	13	10	20	
873	16	5	4	7	
874	14	4	5	5	
875	4	1	1	2	
876	8	3	1	4	
877	6	3	1	2	
878 (b)	86	56	13	17	
878 (v)	106	26	32	48	
879	14	3	6	5	
Total	340	132	81	127	

Notes: (b) = polymictic breccia from Hole 878A, and (v) = volcanic basement from Hole 878A. AF = alternating-field demagnetization. Thermal = thermal demagnetization.

MAD greater or equal to 15° are often considered ill-defined and of questionable significance. The MAD values for most samples from Leg 144 are smaller than 10° (Fig. 1), indicating that the characteristic magnetization directions are generally well defined.

The median destructive field (MDF; the alternating field necessary to reduce the magnetization to 50% of its initial value) provides a first-order measure of the stability of the remanence. The MDFs of most samples are generally between 10 and 40 mT (occasionally > 50 mT; Fig. 2). Figure 3 shows the relation between the MDF and the angular displacement of stable remanence from the NRM direction in individual samples. Samples from Leg 144 typically show little directional change during demagnetization, with a slight negative correlation between these two parameters as has been previously noted (Kono, 1980). For example, the MDFs of the samples that have two components of remanent magnetization (Samples 144-878A-89R-4, 45–47 cm; -91A-4, 138–140 cm; and -98R-3, 46–48 cm, etc.) are small and their angular displacements are large.

The Königsberger ratio (Q; the ratio of remanent to induced magnetization) of igneous rocks also provides some indication of the stability of remanence (Stacey and Banerjee, 1974). With the exception of the polymictic breccia unit of Hole 878A, Q ratios of our samples generally are between 1 and 60 (Fig. 4A). Together with the moderate MDF values and paucity of low-stability secondary magnetization components, the Q ratios suggest that the remanent magnetizations of most of our samples are stable enough to determine the paleolatitudes of the guyots. The Q ratios of polymictic breccia of Hole 878A are smaller than 4, with many samples having values less than unity (Fig. 4B). Thus, remanent magnetizations of polymictic breccia of Hole 878A are not stable enough to estimate a paleolatitude of MIT Guyot.

Pairs of samples from the same core piece were demagnetized, one by AF and the other by thermal treatment. In most cases, AF and thermal demagnetization isolate the same components of magnetization (Fig. 5). Maximum unblocking temperatures in most samples are high (500–650°C), consistent with petrographic evidence for high-temperature oxyexsolution and the presence of secondary hematite in many samples (Gee and Nakanishi, this volume). However, AF demagnetization sometimes resulted in linear demagnetization trends in samples that exhibited erratic behavior during thermal demagnetization (Fig. 6). The MDFs of these samples are smaller than 3 mT.

The results of our shipboard and shore-based paleomagnetic measurements for each guyot are summarized in Tables 3 through 8. Average inclinations for each flow unit are displayed in Table 9. The average inclinations of guyots drilled during Leg 144 are shown in Table 10.

Limalok Guyot

Volcanic basement was drilled to a depth of 48.5 m below the lowest sediment at Hole 871C. We obtained 44 discrete samples for shipboard and shore-based measurements from the volcanic base-

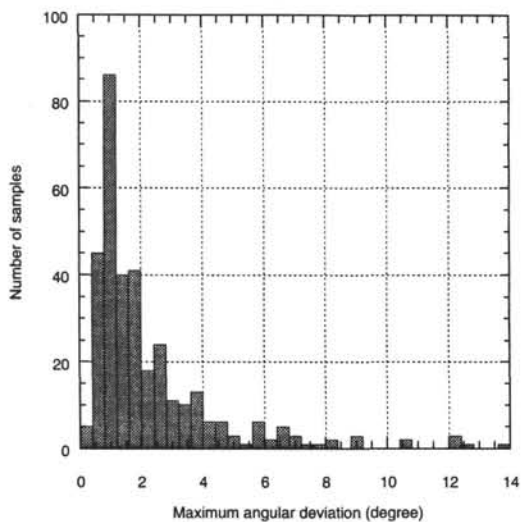


Figure 1. Histogram of maximum angular deviation (MAD) for discrete samples from the volcanic basement of Leg 144 guyots.

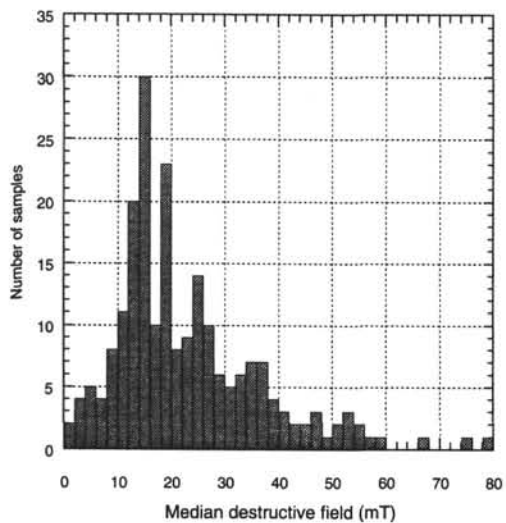


Figure 2. Histogram of median destructive field (MDF) of volcanic rocks from Leg 144.

ment (Fig. 7). Samples shallower than 465 mbsf (Section 144-871C-35R-1) have NRM intensities smaller than 3 Am^{-1} . The intensities of most samples from 470 to 485 mbsf are 1 to 7 Am^{-1} . Below 485 mbsf, NRM intensities of samples from Hole 871C (Sample 144-871C-39R-5, 113–115 cm) gradually increase until they reach 6 Am^{-1} in Sample 144-871C-41R-1, 6–8 cm. The MAD angles of samples from the volcanic basement of this guyot are generally smaller than 6° , whereas the MDFs of the majority of samples are greater than 10 mT. Susceptibilities range from 800 to $5300 \times 10^{-5} \text{ SI}$. Most Q ratios are smaller than 6.

Inclinations of samples from 451.58 to 452.02 mbsf (Section 144-871C-35R-1) are shallower than those in the lower part of the core. Those from 461.46 to 463.08 mbsf (from Samples 144-871C-36R-1, 36–38 cm, to -36R-2, 57–59 cm) are about -30° . Inclinations of the discrete samples below 463.5 mbsf (Sample 144-871C-36R-2, 99–101 cm) range from -10° to -25° . We deleted Samples 144-871C-38R-3, 79–81 cm, and -39R-1, 75–77 cm. Sample 144-871C-38R-3, 79–81 cm, has noisy data from demagnetization and is distinct from the remaining samples in this flow unit. Sample 144-871C-39R-1, 75–77 cm, did not yield a characteristic direction. The mean inclina-

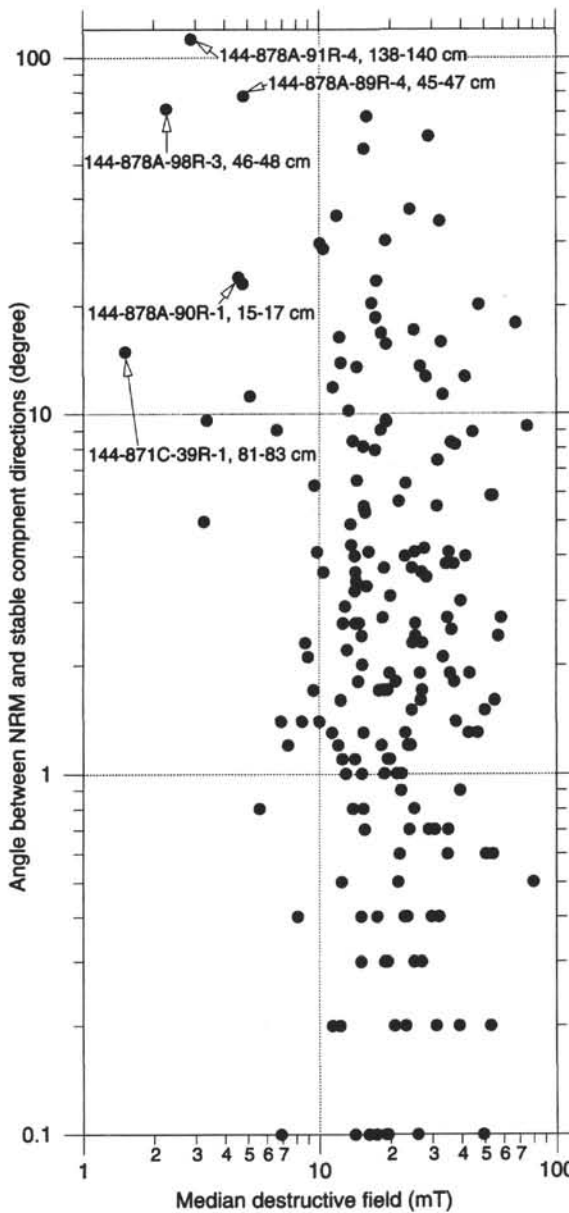


Figure 3. Relation between the MDF and the angular displacement of stable remanence from NRM in individual discrete samples. Angular displacements smaller than 0.1° are plotted at 0.1° .

tion calculated from the 12 flow units recovered on Limalok Guyot is -19.1° ($\alpha = 7.1^\circ$, $k = 37.5$, where α is the half angle of the asymmetric 95% confidence interval and k is the best estimate of κ ; McFadden and Reid, 1982).

Lo-En Guyot

We obtained 43 discrete samples from all three holes of Site 872. The majority of samples are from Hole 872B, which penetrated to a depth of 57.1 m (Fig. 8). Samples shallower than 148 mbsf in Hole 872B are weakly magnetized ($< 3 \text{ Am}^{-1}$). The NRM intensities of samples from 149.79 to 164.12 mbsf (from Samples 144-872B-5R-4, 67–69 cm, to -7R-1, 12–14 cm) are high ($> 6 \text{ Am}^{-1}$). The intensities of samples from 164.29 to 185.82 (from Samples 144-872B-7R-1, 29–31 cm, to -9R-3, 34–36 cm) range from 2 to 9 Am^{-1} . Below 186.58 mbsf (Section 144-872B-9R-4), NRM intensities are much lower ($< 1 \text{ Am}^{-1}$) than the other portions. MADs shallower than 147.63 mbsf

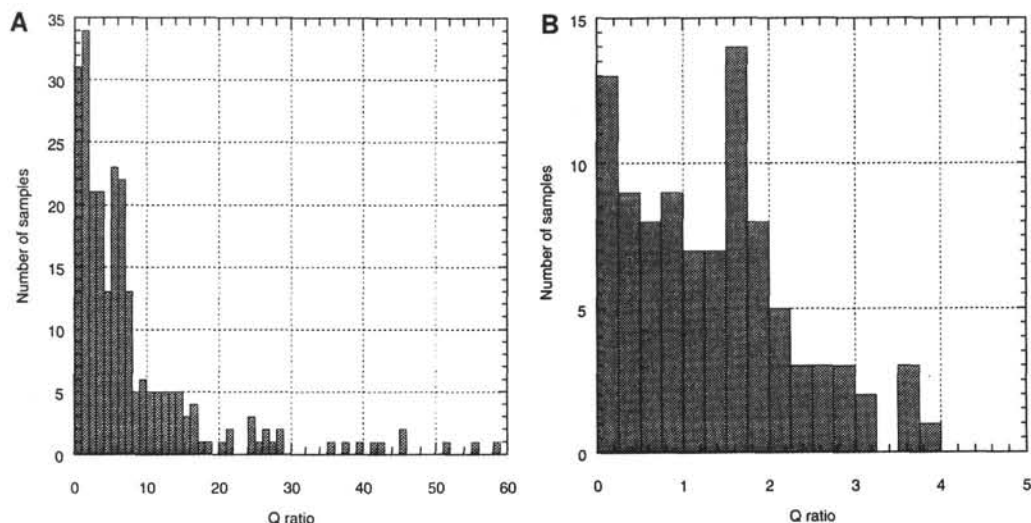


Figure 4. Histograms of Königsberger ratio (Q) of discrete samples from Hole 878A excluding polymictic breccia (A) and of polymictic breccia only (B).

Table 3. AF and thermal demagnetizations from Limalok Guyot.

Core, section, interval (cm)	Depth (mbsf)	Flow unit	Volume (cm³)	Declination (degree)	Inclination (degree)	Intensity (A/m)	MAD (degree)	MDF (mT)	Susceptibility (10⁻⁵ SI)	Q ratio	Demagnetization
144-871C-											
35R-1, 8	451.58	1	10.8	42.3	-11.5	0.37	6.0	—	5234	0.15	AL
35R-1, 29	451.79	1	9.7	132.1	-11.9	2.21	1.8	9.5	2580	3.16	AL
35R-1, 32	451.82	1	8.2	126.0	-1.1	2.71	1.6	2764	3.62	T	
35R-1, 44	451.94	1	9.3	128.0	2.2	1.37	4.0	9.8	3367	0.89	A
35R-1, 52	452.02	1	11.1	126.0	-4.1	1.10	12.2	—	3369	0.71	T
35R-4, 4	455.91	7A	7.5	92.5	-32.6	2.65	1.5	36.0	—	—	A
36R-1, 36	461.46	9	9.3	304.6	-28.3	2.56	2.8	17.3	—	—	A
36R-1, 54	461.64	9	9.9	128.3	-31.5	1.59	1.2	23.0	2816	2.08	AL
36R-1, 58	461.68	9	9.7	121.0	-29.7	1.79	0.6	—	3001	2.20	T
36R-2, 3	462.54	9	7.8	260.9	-35.1	2.97	1.7	22.9	3447	1.88	AL
36R-2, 57	463.08	10	9.0	235.2	-33.3	1.00	4.5	41.5	—	—	A
36R-2, 99	463.50	13	9.2	348.4	-13.0	1.26	0.7	—	1077	4.30	T
36R-2, 103	463.54	13	10.2	351.2	-14.7	1.20	1.6	19.1	1078	4.12	AL
36R-3, 17	464.11	13	9.8	80.2	-22.2	2.12	12.6	—	835	5.54	T
36R-3, 25	464.19	13	9.3	260.2	-18.3	2.81	2.8	15.7	941	6.51	A
36R-3, 38	464.32	13	11.0	81.0	-13.8	1.68	12.2	—	1974	1.86	T
37R-1, 52	470.32	15	10.2	73.4	-14.5	3.24	1.2	27.3	4148	2.88	AL
37R-1, 65	470.45	15	10.7	74.5	-11.4	6.46	0.6	—	4271	5.59	T
37R-1, 85	470.65	15	10.2	279.6	-6.2	5.97	1.4	24.4	—	—	A
37R-1, 129	471.09	15	8.6	263.8	-8.9	3.32	1.8	—	4225	1.71	T
37R-2, 11	471.38	15	10.6	130.2	-7.0	2.01	10.7	—	4098	1.07	T
37R-2, 16	471.43	15	10.2	132.6	-6.0	3.22	2.4	17.4	—	—	A
37R-2, 87	472.14	16	10.2	176.5	-8.0	16.80	0.7	19.2	—	—	A
38R-1, 73	472.53	17	10.6	132.0	-12.7	1.67	1.1	—	1812	2.01	AL
38R-1, 85	472.65	17	9.8	160.9	-15.7	1.63	4.9	11.9	—	—	A
38R-2, 101	474.17	17	10.2	43.0	-24.4	1.65	0.8	10.4	2416	2.53	AL
38R-2, 104	474.20	17	9.5	40.2	-20.5	2.34	1.8	—	2613	3.31	T
38R-3, 79*	475.45	17	9.6	126.0	-42.5	2.86	6.1	—	1572	3.97	T
38R-3, 84	475.50	17	9.1	119.3	-19.4	4.28	3.3	9.0	1577	5.92	A
38R-5, 56	478.01	19	9.3	195.1	-15.8	2.48	1.3	15.3	—	—	A
38R-6, 13	478.52	19	9.5	280.8	-16.3	2.21	0.9	—	1844	4.42	T
38R-6, 17	478.56	19	8.7	283.2	-20.1	2.58	1.4	12.6	1929	4.94	AL
38R-6, 96	479.35	19	9.3	144.7	-21.9	3.17	1.5	12.3	—	—	A
38R-6, 97	479.36	19	10.8	146.4	-23.7	3.02	8.4	—	2200	2.99	T
39R-1, 75*	481.15	21	10.1	—	—	1.43	—	—	2304	1.35	T
39R-1, 81	481.21	21	10.6	227.5	-22.3	17.76	2.7	1.5	2654	14.59	A
39R-2, 46	482.17	21	6.8	255.2	-18.2	2.89	2.9	10.5	2988	3.57	AL
39R-2, 50	482.21	21	8.4	251.0	-14.8	2.71	1.5	—	3039	3.29	T
39R-4, 11	484.59	21	10.4	234.3	-19.5	10.11	0.7	19.4	4216	5.23	A
39R-5, 113	487.11	21	9.4	291.6	-20.4	2.73	1.8	37.1	—	—	A
39R-6, 118	488.66	22	0.0	153.4	-17.7	3.45	2.5	37.8	4791	1.57	A
39R-6, 122	488.70	22	10.2	156.0	-17.8	3.53	5.8	—	4042	1.90	T
40R-1, 141	491.11	22	10.9	85.1	-18.3	4.50	0.9	32.1	4937	1.99	A
40R-4, 52	494.72	22	10.0	257.9	-11.6	4.17	1.3	—	2832	3.21	T
40R-4, 62	494.82	22	10.2	243.7	-13.2	5.72	1.3	24.6	—	—	A
41B-1, 6	496.00	23	10.2	218.5	-17.9	5.63	6.8	3.3	436	28.18	A

Notes: MAD = maximum angular deviation, and MDF = median destructive field. A = shipboard AF demagnetization, AL = shore-based AF demagnetization, and T = shore-based thermal demagnetization. An asterisk (*) = sample excluded from calculation of an average inclination, blanks = not applicable, and dashes = no data.

(Section 144-872B-5R-3) are scattered. Those below 149.12 mbsf (Section 144-872B-5R-4) are smaller than 2°. Susceptibilities are generally less than 4000×10^{-5} SI. Most Q ratios for samples from Lo-En Guyot are larger than those of samples from Limalok Guyot.

Most samples from Lo-En Guyot have inclinations from -60° to -40°. A small number of samples (Table 4) have positive inclinations, which we interpret as resulting from accidental inversion of core

pieces during sampling or curation. With the exception of Sample 144-871C-7R-2, 57–59 cm (a flow-top breccia with a significantly different inclination than the remainder of the flow), all samples were included in calculating flow mean inclinations. The resulting mean inclinations for 11 flow units yield an average inclination for Lo-En Guyot of -49.8° ($\alpha = 5.4^\circ$, $k = 72.6$), which we interpret as a normal polarity magnetization acquired in the Southern Hemisphere.

Table 4. AF and thermal demagnetizations from Lo-En Guyot.

Core, section, interval (cm)	Depth (mbsf)	Flow unit	Volume (cm ³)	Declination (degree)	Inclination (degree)	Intensity (A/m)	MAD (degree)	MDF (mT)	Susceptibility (10 ⁻⁵ SI)	Q ratio	Demagnetization
144-872A-											
18X-1, 19	143.89	1	10.7	332.2	-40.6	2.78	3.1	2149	2.82	T	
18X-1, 22	143.92	1	11.5	204.6	-24.1	2.33	4.6	2124	2.39	AL	
144-872B-											
5R-1, 26	145.06	6	11.1	152.0	-50.2	2.31	1.6	13.2	1437	5.89	AL
5R-1, 29	145.09	6	10.9	72.1	-46.2	1.87	0.8	1248	5.50	T	
5R-1, 47	145.27	6	0.0	76.4	-47.3	1.61	1.6	18.3	1729	2.03	A
5R-1, 54	145.34	6	9.4	142.5	-45.8	2.71	6.9	1845	3.20	T	
5R-3, 11	147.73	9A	10.4	23.5	-50.5	2.21	1.4	24.0	566	14.32	AL
5R-3, 14	147.76	9A	10.4	19.1	-51.9	2.45	0.6	—	548	16.38	T
5R-3, 98	148.60	9B	9.5	97.5	-51.0	1.22	3.7	—	314	8.48	T
5R-3, 102	148.64	9B	0.0	99.6	-42.3	1.53	2.2	16.1	442	7.55	A
5R-4, 67	149.79	10B	8.2	340.5	-49.2	10.44	0.6	—	3918	9.77	T
5R-4, 70	149.82	10B	8.2	336.9	-49.7	8.49	0.8	21.8	2403	12.96	AL
6R-1, 40	154.90	10B	0.0	180.9	-48.0	7.71	1.2	29.0	2784	6.04	A
6R-1, 43	154.93	10B	9.4	174.4	-50.6	6.20	0.7	—	1846	7.32	T
7R-1, 9	164.09	13	7.3	310.0	-45.7	4.28	0.6	—	1346	11.65	T
7R-1, 12	164.12	13	9.7	307.0	-45.2	4.15	1.1	19.6	1310	11.61	AL
7R-1, 29	164.29	13	9.4	313.2	-45.3	2.82	1.1	—	1074	5.73	T
7R-1, 31	164.31	13	11.7	313.9	-43.3	3.52	0.9	19.9	1442	5.32	A
7R-2, 57*	165.22	14A	10.8	142.0	-33.5	12.42	1.8	18.7	3938	6.88	AL
7R-3, 113	167.05	14A	9.7	336.6	-48.4	5.06	0.5	—	3366	3.28	AL
7R-4, 67	168.09	14B	11.7	94.4	-56.5	4.64	1.1	31.3	2705	3.74	A
7R-4, 87	168.29	14B	9.2	261.1	-56.3	3.64	1.8	—	1898	4.18	T
7R-4, 125	168.67	14B	9.7	8.5	-56.0	2.68	0.8	33.3	1553	6.34	AL
7R-7, 50	172.13	15B	10.7	167.7	-54.7	4.98	0.9	—	1369	13.35	T
7R-7, 54	172.17	15B	10.9	177.5	-54.6	5.08	0.9	21.9	1486	12.53	AL
7R-7, 68	172.31	15B	9.5	289.9	-50.9	4.86	1.3	—	1687	6.28	T
7R-7, 74	172.37	15B	11.7	289.0	-48.7	4.42	1.0	19.8	1904	5.06	A
8R-1, 70	173.80	16A	9.3	311.2	-51.7	8.46	0.3	21.6	—	—	A
8R-2, 87	175.33	16B	9.5	89.4	-40.7	3.04	7.8	—	4330	1.53	T
8R-2, 89	175.35	16B	10.6	90.8	-43.4	2.79	1.2	10.4	—	—	A
8R-2, 139	175.85	16B	9.7	270.7	-44.7	2.50	0.9	12.0	6018	1.52	AL
8R-4, 6	177.48	16B	9.7	235.9	-54.7	4.81	0.4	—	46.5	—	A
8R-4, 43	177.85	16B	10.7	142.8	-51.8	5.91	0.9	30.8	1338	9.63	A
9R-1, 24	182.84	17A	7.3	157.7	-60.7	3.28	1.9	—	708	16.97	T
9R-2, 89	184.87	17B	9.7	98.5	-59.0	4.53	1.5	—	1871	5.28	T
9R-2, 92	184.90	17B	9.7	99.4	-61.0	6.23	2.3	—	8.5	—	A
9R-3, 29	185.77	17B	9.7	57.9	-58.8	3.80	0.4	37.8	1043	13.38	AL
9R-3, 34	185.82	17B	10.2	71.5	-60.5	2.83	1.1	—	1682	6.16	T
9R-4, 56	187.14	18B	9.7	—	—	0.13	—	—	44	10.74	A
9R-5, 131	189.29	18B	9.7	274.4	-53.6	0.23	2.0	—	—	—	A
9R-5, 136	189.34	18B	9.5	87.0	-51.2	0.31	1.1	—	110	6.06	T
9R-6, 4	189.46	18B	11.3	82.3	-32.3	0.27	0.7	—	73	8.08	AL
9R-6, 8	189.50	18B	9.7	79.7	-57.2	0.61	1.0	—	90	24.66	T
144-872C-											
18X-1, 95	146.95	1	9.9	34.6	-39.7	1.30	1.1	—	481	9.90	T
18X-1, 98	146.98	1	10.2	31.5	-40.4	1.17	0.5	19.4	428	10.00	AL
18X-2, 26	147.62	1	0.0	144.0	-49.4	7.11	0.4	—	—	—	A
18X-2, 30	147.66	1	10.3	137.3	-52.1	2.29	0.8	—	389	12.85	T

Notes: Abbreviations and symbols as in Table 3.

Wodejebato Guyot

Although the deepest basement penetration on Wodejebato Guyot was ~50 m (Table 1), some volcanic material was recovered at each of five sites (Sites 873–877). Figures 9 and 10 illustrate the depth variation of paleomagnetic parameters for samples from the two deepest holes (Holes 873A and 874B). The NRM intensities of samples shallower than 203.74 mbsf (Sample 144-873A-18R-1, 74–76 cm) are from 2.78 to 8.05 Am⁻¹. Samples 144-873A-18R-1, 91–93 cm, 97–99 cm, and 124–126 cm, are greater than 12 Am⁻¹. Samples below 216.61 mbsf (Core 144-873A-19R), which are from a volcanic breccia, have very weak magnetizations (<1 Am⁻¹). The NRM intensities of samples of the volcanic basement from Hole 874B range from 1 to 9 Am⁻¹. At Hole 875C, the upper portion of Section 144-875C-15M-1 has NRM intensities smaller than 1 Am⁻¹, but the lower portion has intensities of 4 to 6 Am⁻¹. Intensities of Samples 144-877A-20R-4, 111–113 cm and 115–117 cm, and -20R-5, 19–21 cm, are greater than 10 Am⁻¹, and those of three other samples from Hole 877A are 1.09 to 2.25 Am⁻¹. Most of the samples from Wodejebato Guyot have MAD angles smaller than 3°. The susceptibilities of samples from Hole 873A are generally less than 1500 × 10⁻⁵ SI. The Q ratios of samples from the lower part of Hole 874B are larger than those from the upper part.

Inclinations of the volcanic basement from Wodejebato Guyot range from -7.1° to 53.2° (Table 5). The top three samples taken from the flow-top breccia of the ankaramitic flow(s) sampled at Site 874 (Samples 144-874B-22R-4, 17–19 cm; -22R-4, 32–34 cm; and -23R-1, 28–30 cm) were excluded because they are extensively altered

(Gee and Nakanishi, this volume). We also excluded the volcanic breccia samples from the top of Hole 877A (Samples 144-877A-20R-1, 23–25 cm; -20R-2, 72–74 cm; and -20R-3, 25–27 cm) because their inclinations are internally inconsistent. Although Unit 9 of Hole 873A is a pyroclastic bomb, samples from this flow unit have the same inclination as the adjacent units. This implies that the unit has cooled and acquired a remanence during or shortly after deposition. Samples from Sites 875 to 876 on the outer perimeter ridge of Wodejebato Guyot have somewhat shallower inclinations than elsewhere on the guyot and include two samples with negative inclinations. Although these data might be taken as evidence for some normal polarity material on this predominantly reversed polarity guyot, the substantial number of samples that have been demonstrably inverted during sampling precludes resolution of this question. We interpret the positive inclination of this guyot as representing a reversed polarity magnetization acquired in the Southern Hemisphere. Radiometric age determinations for Wodejebato Guyot range from 79 to 85 Ma (Pringle et al., this volume), compatible with a reversed polarity remanence acquired during Chron C33R. The average inclination of Wodejebato Guyot is 16.5° ($\alpha = 8.3^\circ$, $k = 30.3$).

MIT Guyot

Hole 878A penetrated 185.26 m into the volcanic basement of MIT Guyot (722.54–907.80 mbsf). In addition, a polymictic breccia (399.74–604.3 mbsf) rich in volcanic material was also sampled at this hole. These two units are separated by a limestone with an early Aptian paleontologic age. We obtained 86 and 106 samples from the

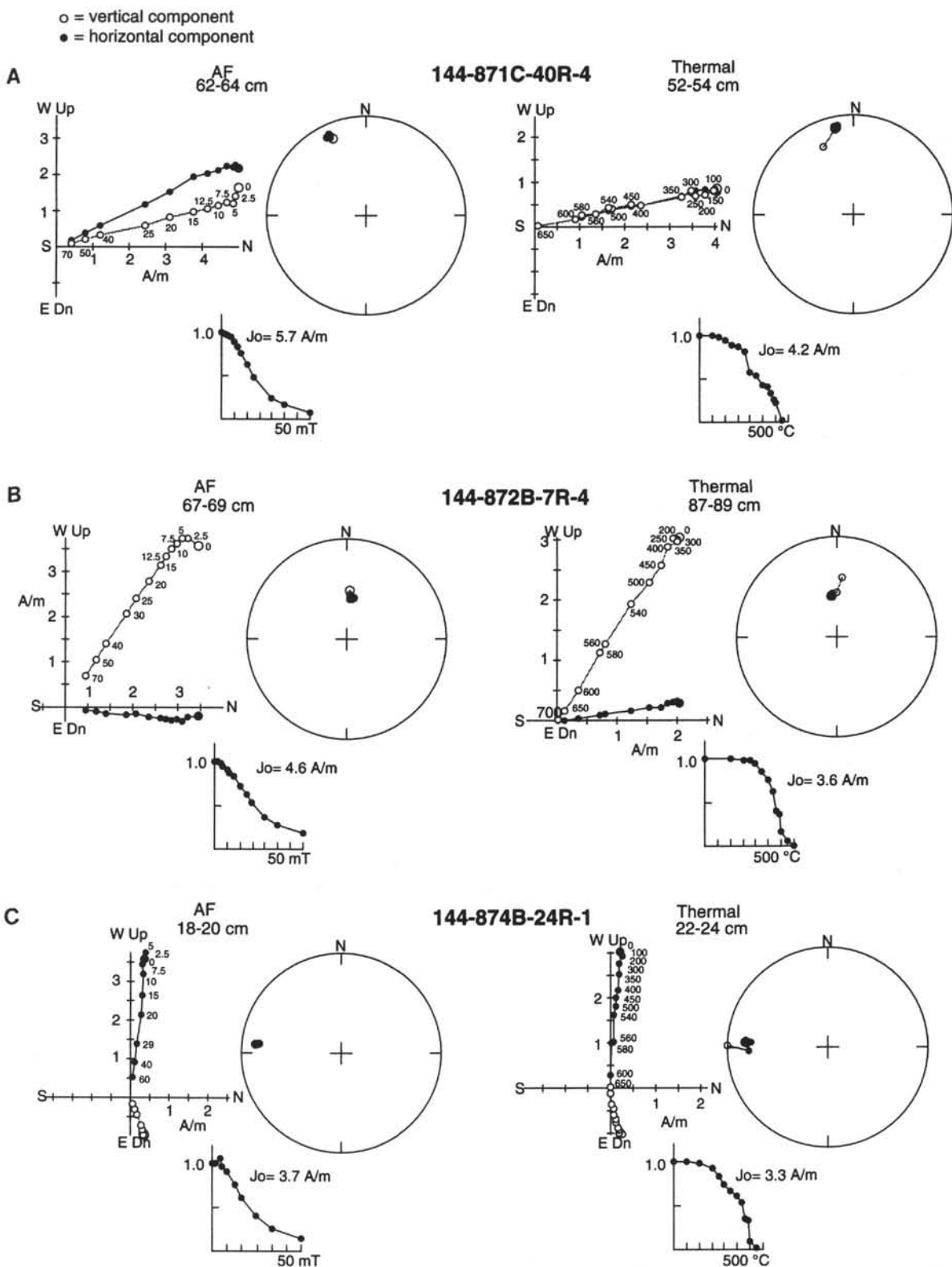


Figure 5. Vector projection diagram and stereographic (equal-area) projection of successive demagnetization steps on samples from (A) Limalok Guyot (Site 871), (B) Lo-En Guyot (Site 872), (C) Wodejebato Guyot (Site 874), (D) MIT Guyot (Site 878), and (E) Takuyo-Daisan Guyot (Site 879).

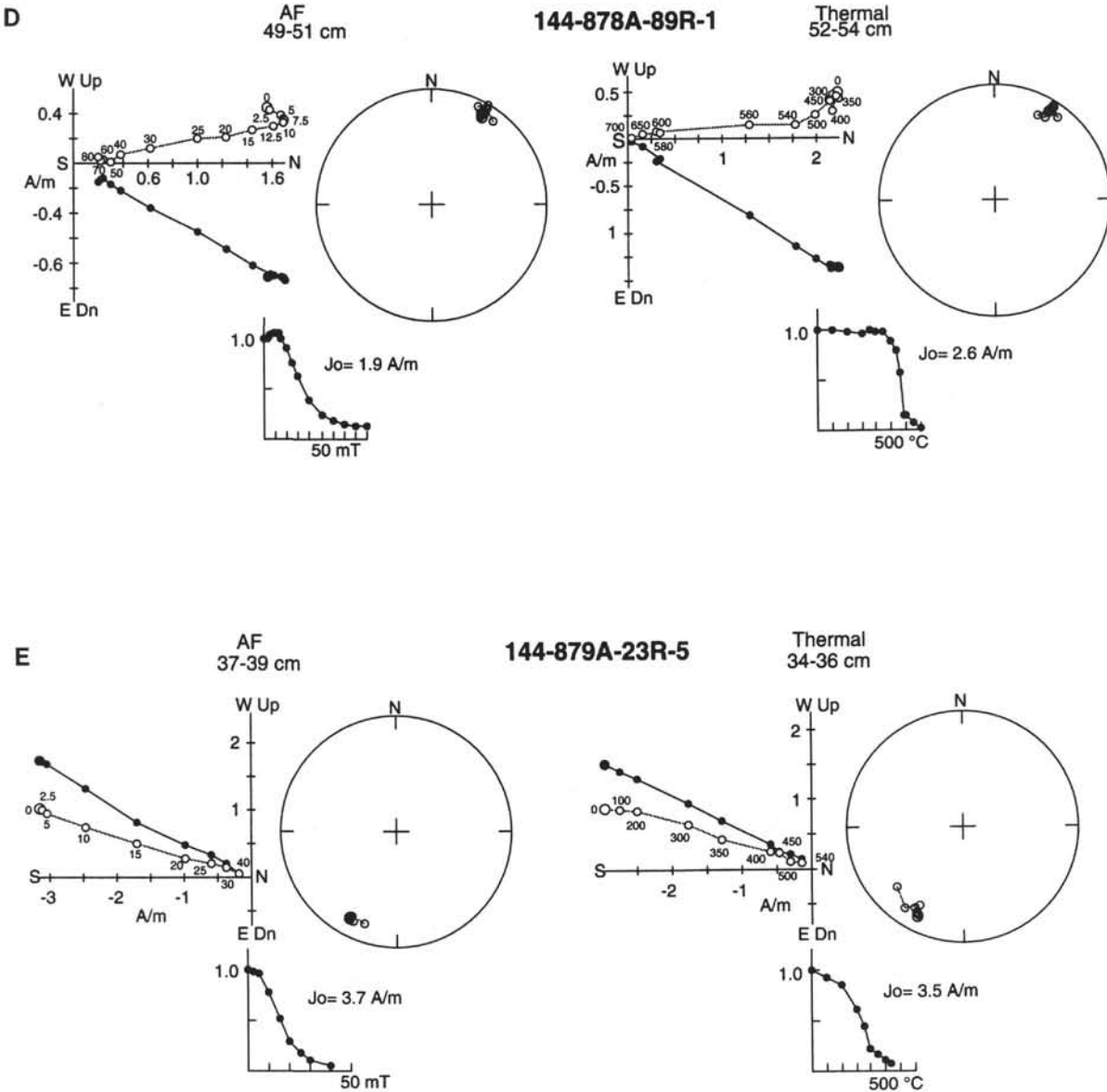


Figure 5 (continued).

volcanic basement and the polymictic breccia, respectively. Moreover, we conducted shipboard whole-core remanence measurements on the archive halves of cores from the volcanic basement and polymictic breccia.

Polymictic Breccia

Figure 11 displays paleomagnetic parameters of the polymictic breccia from Hole 878A as a function of depth. Most of the samples of the polymictic breccia are weakly magnetized, with NRM smaller than 0.1 Am^{-1} . The MDFs of the samples from the polymictic breccia are smaller ($<20 \text{ mT}$) than those of the volcanic basement. Susceptibilities are not greater than $100 \times 10^{-5} \text{ SI}$. Most of the Q ratios are smaller than 2. Maximum unblocking temperatures in samples of the polymictic breccia are low. The average inclination of discrete samples is -39.2° ($\alpha = 1.2^\circ$, $k = 21.2$). The magnetic record obtained from the archive halves of cores of the polymictic breccia from Hole 878A after AF demagnetization at 15 mT as well as those of discrete samples is shown in Figure 12. The peak of inclination by whole-core measurements is -38° to -46° (Fig. 13) and is consistent with the average inclination determined from discrete sample demagnetiza-

tion data. Although the normal polarity of this unit is well established, the erratic behavior of some samples during demagnetization and the discrepancies between immediately adjacent samples suggest that the geologic significance of the inclination data from the polymictic breccia unit is uncertain.

Volcanic Basement

The NRM intensities of the volcanic basement of Hole 878A are scattered (Fig. 14). The maximum NRM intensity is 12.7 Am^{-1} . Samples from 820.71 to 857.21 mbsf (from Sections 144-878A-88R-3 to -92R-1) are weakly magnetized, with NRM intensities smaller than 1 Am^{-1} . The MAD angles of the volcanic basement are generally smaller than 4° . Some samples have large MDFs, greater than 40 mT. Most susceptibilities are smaller than $6000 \times 10^{-5} \text{ SI}$. The Q ratios of most of them are smaller than 10.

Both the magnetic record obtained from the archive halves of core from the volcanic basement in Hole 878A after AF demagnetization at 15 mT as well as data obtained from discrete samples reveal the presence of normal and reversed polarity material (Fig. 15). The polarity of samples shallower than 800 mbsf (Core 144-878A-86R)

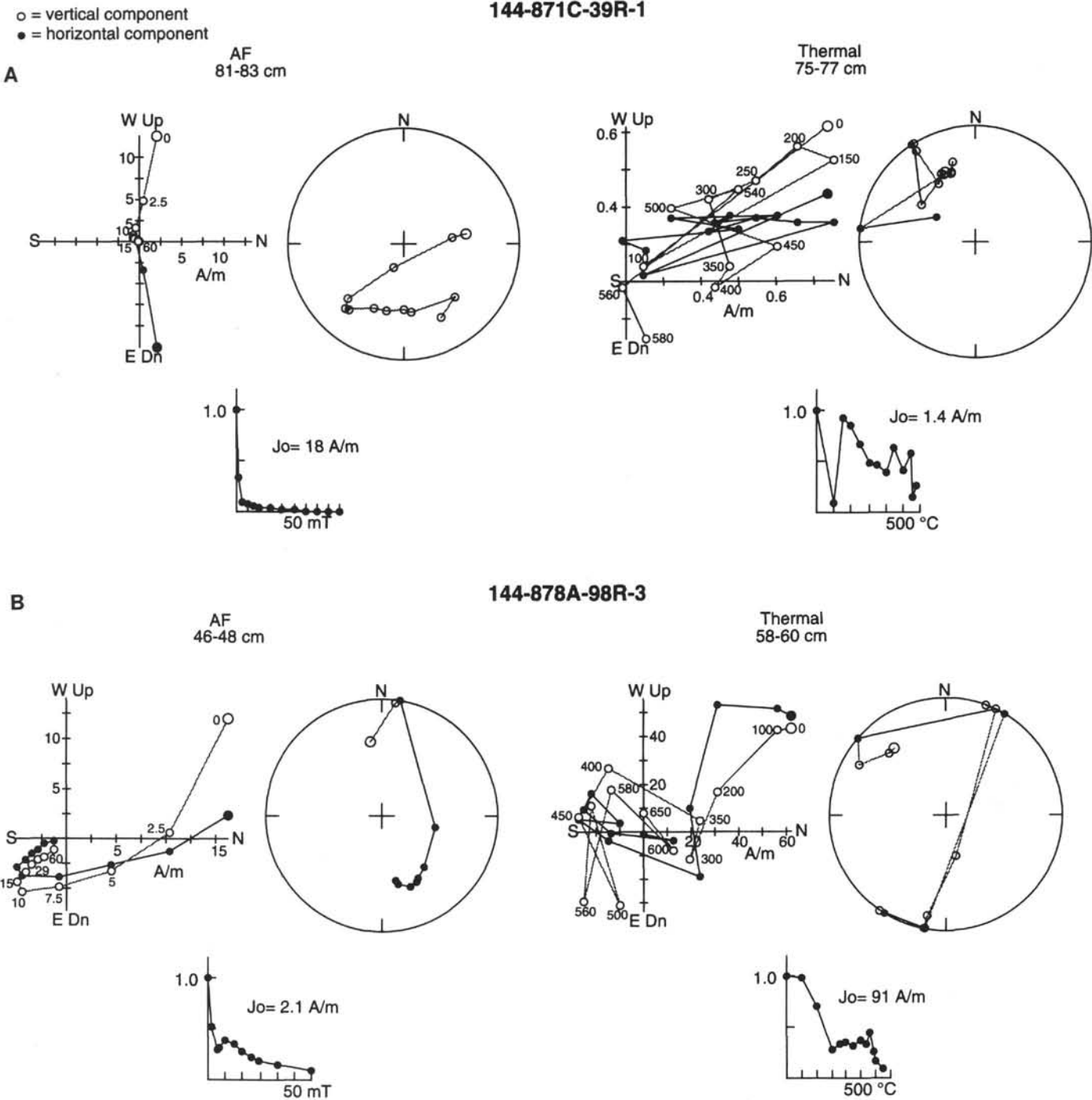


Figure 6. Vector projection diagram and stereographic (equal-area) projection of successive demagnetization steps on samples from (A) Limalok Guyot and (B) MIT Guyot, in which thermal demagnetization produced erratic behavior whereas AF demagnetization resulted in linear demagnetization trends. Indicators same as Figure 5.

is normal and that below 838.46 mbsf (Section 144-878A-90R-4) is reversed. The intervening zone (801.6 through 838.9 mbsf) contains samples with shallow inclinations (Unit 21) as well as two samples from Unit 18 that have positive inclinations. The latter two samples (Samples 144-878A-86R-3, 39-41 cm and 43-45 cm) were taken from a single core piece and so accidental inversion of this piece cannot be excluded. This zone of indeterminate polarity, which might plausibly represent transitional field behavior, was excluded from calculation of the mean inclination for the guyot.

Inclinations of discrete samples with a normal polarity range from -11° to -42° , whereas those of discrete samples with a reversed

polarity range from -1° to 40° . Most of samples with an intermediate polarity have shallower inclinations ($<10^\circ$). The average inclination of the samples with a normal polarity is -22.2° ($\alpha = 7.3^\circ$, $k = 44.4$), whereas that of reversed polarity samples is 22.0° ($\alpha = 5.7^\circ$, $k = 50.8$). The average inclination of the volcanic basement, combining both polarities from MIT Guyot, is -22.1° ($\alpha = 4.1^\circ$, $k = 50.1$). Figure 16 shows a histogram of inclinations obtained from the whole-core measurement. The peak inclinations of the histogram are -6° to -14° and 18° to 26° , inconsistent with the average inclinations determined from the discrete sample data. This probably reflects the inadequacy of the 15-mT AF demagnetization to isolate the characteristic rema-

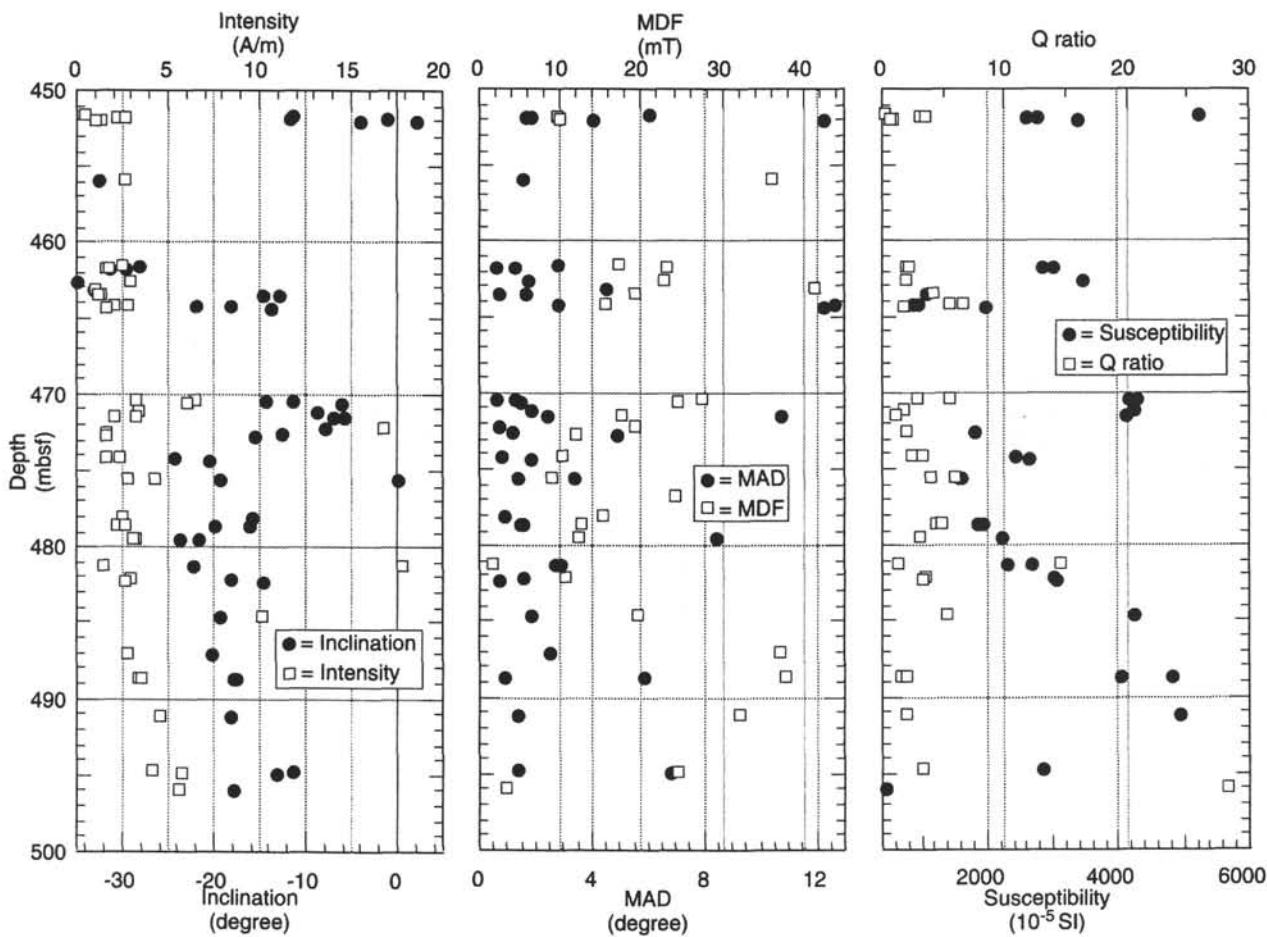


Figure 7. Paleomagnetic parameters, inclinations, NRM intensities, MADs, MDFs, susceptibilities, and Q ratios of Hole 871C vs. depth.

nence in the archive half data. Most of their MDFs for the discrete samples are greater than 20 mT (Fig. 14), providing further support for this interpretation.

The radiometric age of volcanic rocks from MIT Guyot (122.9 ± 0.9 Ma; Pringle et al., this volume) implies that the reversed polarity corresponds to Chron M1 or older. Shore-based measurement of discrete samples of the limestone between the polymictic breccia and the volcanic basement of Hole 878A could not confirm whether a polarity of the limestone is normal or reversed (Nakanishi et al., 1993). Thus, we cannot definitively say which chron corresponds to the reversed polarity of the volcanic basement of Hole 878A.

Takuyo-Daisan Guyot

Drilling at Takuyo-Daisan Guyot penetrated ~35 m into the volcanic basement, yielding 14 discrete samples for both shipboard and shore-based measurements (Fig. 17). The NRM intensities range from 2 to 5 Am⁻¹ except for samples from Section 144-879A-23R-1, which have intensities smaller than 1 Am⁻¹. The MADs of most samples are smaller than 2°. Most MDFs are greater than 20 mT. Susceptibilities range from 100 to 600×10^{-5} SI. Maximum unblocking temperatures for most samples are smaller than 540°C (Fig. 5E) and are somewhat lower than those of samples from other guyots. The Q ratios are less than 50.

Stepwise AF and thermal demagnetizations of all the samples yield an average inclination of the volcanic basement of Takuyo-Daisan Guyot of -19.2° ($\alpha = 6.0^\circ$, $k = 42.6$), which is nearly the same as that obtained from samples taken at Limalok Guyot. Results from archive half-core measurements and discrete samples from the vol-

canic basement are shown in Figure 18. Figure 19 illustrates the histogram of inclinations obtained from the whole-core measurement. The peak inclinations of the histogram are -8° to -12° . The peak is different from the average inclination of this guyot, which is similar to conditions found at MIT Guyot. The MDFs of samples from Takuyo-Daisan Guyot are mostly greater than 20 mT (Fig. 17).

PALEOLATITUDES OF GUYOTS

Paleolatitudes from the combined shipboard and shore-based data are generally compatible with the preliminary shipboard paleolatitude estimates. The paleolatitude ϕ was calculated by the dipole formula:

$$\tan \phi = (1/2)\tan I, \quad (1)$$

where ϕ is a paleolatitude and I is the average inclination for a guyot. Despite the range of ages and present-day latitudes, the paleolatitudes of four of the five guyots drilled during Leg 144 are all $\sim 10^\circ$ S (Table 10). The average inclination of Lo-En Guyot indicates formation at approximately 31° S. Although the average inclination values for all five guyots provide valuable constraints on the latitude of seamount formation and past motions of the Pacific Plate, the shallow depths of basement penetration (Table 1) may not have sampled a sufficient number of flow units to provide a good estimate of the time-averaged geomagnetic inclination.

Models of paleosecular variation based on the characteristics of the recent geomagnetic field provide an estimate of the expected directional scatter at the latitude of seamount formation. We have used the paleosecular variation model of McFadden et al. (1988), based on data from lavas over the past 5 m.y., to calculate the expected

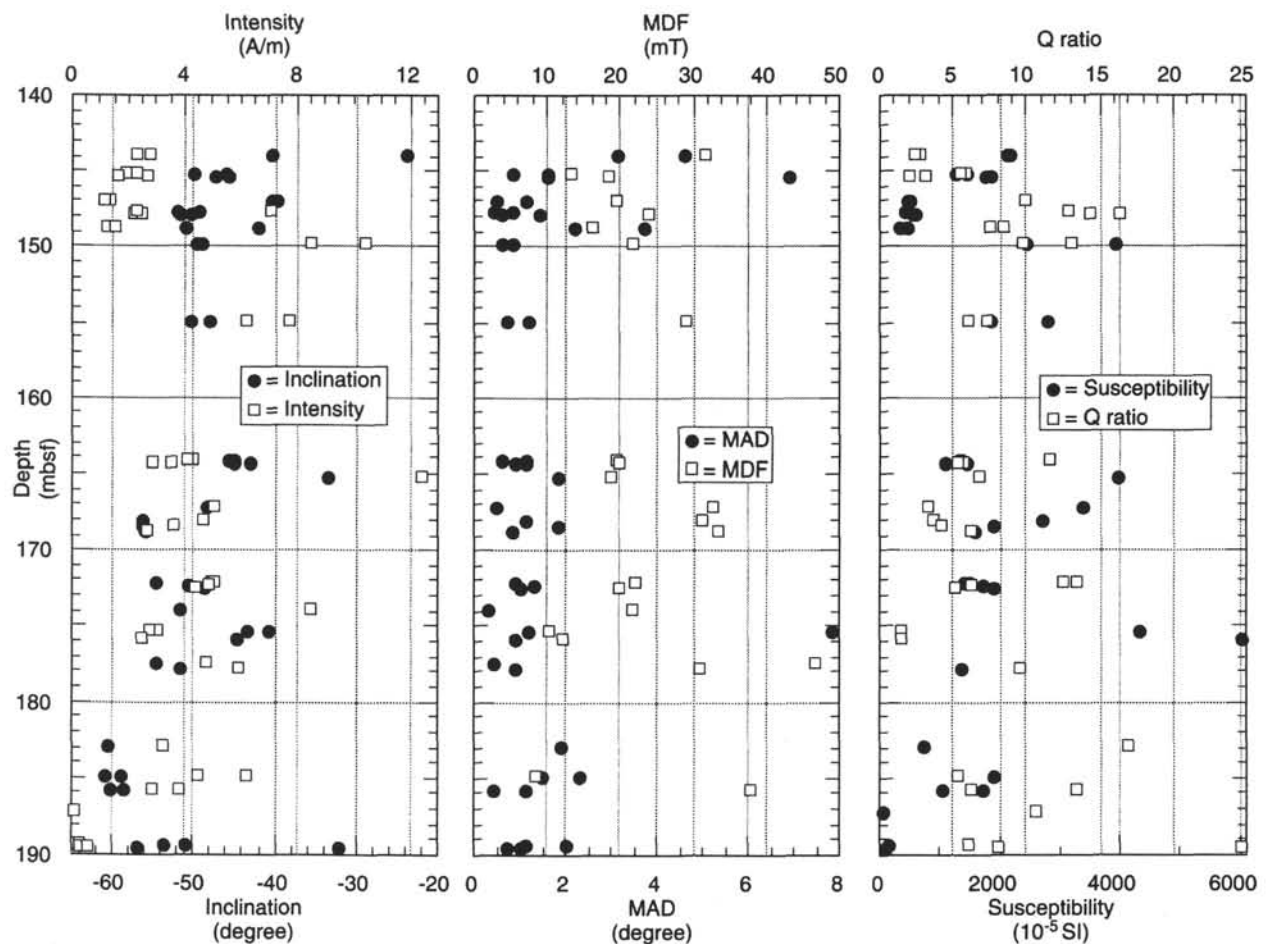


Figure 8. Paleomagnetic parameters, inclinations, NRM intensities, MADs, MDFs, susceptibilities, and Q ratios of Site 872 vs. depth.

directional scatter (and equivalent k) for each guyot from Leg 144 (Table 10). The values of k for all guyots sampled during Leg 144 are higher than those predicted from the paleosecular variation model. The one-sided F test of McFadden (1980), with $N - 1$ degrees of freedom appropriate for inclination-only data (McFadden and Reid, 1982), indicates that Limalok and Wodejebato guyots have k values that are statistically indistinguishable from the expected k at the 95% confidence level. Therefore, the paleolatitude values from these two guyots may have adequately averaged paleosecular variation. In addition, the recovery of volcanic material from five sites on the summit of Wodejebato Guyot approaches the number of sites in some land-based paleomagnetic studies, providing additional support for the validity of this paleolatitude estimate.

Inclination data from Lo-En and MIT guyots have k values that are statistically distinct from the expected values. Although the relatively small number of flow units sampled on Lo-En Guyot may not have adequately averaged paleosecular variation, the apparent lack of time averaging at MIT Guyot is surprising, given the presence of both normal and reversed polarity material. The mean inclinations and k values for the normal and reversed polarity lavas at Site 878 are statistically indistinguishable at the 95% confidence level, providing strong support for the validity of the paleolatitude estimate for the guyot. The higher than expected k values for lavas from MIT Guyot may reflect the time averaging inherent in later alteration and acquisition of a chemical remanence (e.g., Van Fossen and Kent, 1993) or may be indicative of lower paleosecular variation in the Early Cretaceous. Paleosecular variation during the Mesozoic, and particularly within the Cretaceous long normal period, may have been somewhat

lower than values determined for the recent geomagnetic field (e.g., Irving and Pullaiah, 1976).

The paleolatitude of the polymictic breccia in Hole 878A from the average inclination of discrete samples is 22.2°S. The age of the polymictic breccia is early to late Aptian (Premoli Silva, Haggerty, Rack, et al., 1993). The difference between the paleolatitude determined by the volcanic basement (11.4°S) and that inferred for the polymictic breccia is large (11°) and is difficult to reconcile with previous studies of Pacific Plate motion (e.g., Duncan and Clague, 1985). Although average inclinations from discrete samples and archive-half remanence measurements are similar, the geologic significance of the inclination data from this unit is uncertain. Logging data indicate that Hole 878A deviated approximately 4° to 5° from the vertical (toward 170°). This southerly deviation would result in a slightly higher than average inclination for MIT Guyot than that reported in Table 10.

The single flow unit recovered at Takuyo-Daisan Guyot shows significant scatter in inclination values (-2° to -38°); however, the amount of time represented by this unit (amoeboidal pillows that apparently erupted into soft sediment) is unknown. Furthermore, logging results indicate a substantial deviation of the hole from vertical ($\sim 10^{\circ}$, azimuth 300°; Premoli Silva, Haggerty, Rack, et al., 1993). The effect of the deviation from vertical on the paleolatitude of Takuyo-Daisan Guyot depends strongly on the declination of NRM. With no independent control on declination, we have not attempted to correct the paleolatitude data. This 10° deviation from vertical and the presence of only a single flow unit at Site 879 suggest that the paleolatitudinal estimate for Takuyo-Daisan Guyot may be poorly constrained.

Table 5. AF and thermal demagnetizations from Wodejebato Guyot.

Core, section, interval (cm)	Depth (mbsf)	Flow unit	Volume (cm ³)	Declination (degree)	Inclination (degree)	Intensity (A/m)	MAD (degree)	MDF (mT)	Susceptibility (10 ⁻⁵ SI)	Q ratio	Demagnetization
144-873A-											
15R-1, 23	177.63	4	11.8	348.1	23.4	4.13	1.2	—	5601	2.86	T
17R-1, 50	194.30	7	7.9	24.3	25.5	4.33	1.0	6985	1.47	T	T
18R-1, 10	203.10	8	8.7	297.8	25.3	2.78	2.3	—	—	—	A
18R-1, 19	203.19	8	9.1	305.4	26.9	4.45	1.7	4.8	—	—	T
18R-1, 62	203.62	8	9.2	221.1	14.3	8.05	0.5	—	538	55.23	T
18R-1, 66	203.66	8	7.3	219.3	16.6	3.00	0.8	27.1	310	35.75	AL
18R-1, 74	203.74	8	10.3	357.6	20.8	8.04	1.1	19.4	826	21.23	AL
18R-1, 91	203.91	8	10.6	301.5	16.7	12.88	1.3	—	—	—	A
18R-1, 97	203.97	8	9.5	297.6	20.2	14.80	1.2	—	861	37.48	T
18R-1, 124	204.24	8	8.7	—	2.7	15.2	15.83	0.6	1001	58.47	AL
19R-4, 104	217.65	9	11.3	287.3	24.2	0.13	2.5	19.1	—	—	A
21R-1, 61	228.81	9	8.7	26.8	21.4	0.79	1.4	18.8	721	4.04	AL
21R-1, 65	228.85	9	8.5	34.6	20.8	1.01	0.9	—	675	5.53	T
21R-1, 121	229.41	9	10.6	27.9	19.9	0.87	6.0	—	801	2.38	T
21R-1, 126	229.46	9	10.9	19.7	18.7	0.95	0.6	19.4	—	—	A
21R-2, 26	229.89	9	9.7	217.8	18.0	0.97	0.6	—	668	5.38	T
21R-2, 29	229.92	9	7.3	220.9	19.0	0.77	1.4	17.2	765	3.74	AL
21R-2, 109	230.72	9	10.3	20.6	20.6	0.36	2.8	12.9	639	1.24	AL
144-874B-											
22R-4, 17*	176.84	1	10.7	334.6	53.2	1.36	0.9	—	953	5.29	T
22R-4, 32*	176.99	1	8.8	323.7	36.4	3.60	0.7	23.5	998	7.87	AL
23R-1, 28*	177.98	1	8.7	30.0	36.5	2.65	0.8	—	1602	6.11	T
23R-3, 2	180.73	1	11.8	17.7	20.9	2.11	1.3	26.6	2558	1.80	AL
23R-3, 40	181.11	1	10.8	35.3	19.3	3.83	0.8	33.4	2837	2.94	A
24R-1, 18	184.18	1	9.9	186.1	16.8	3.70	1.4	24.7	967	8.35	A
24R-1, 22	184.22	1	9.9	183.9	21.0	3.27	1.2	—	998	7.15	T
24R-1, 47	184.47	1	9.7	229.2	23.3	3.53	0.9	—	1075	12.12	T
24R-1, 51	184.51	1	9.2	228.9	21.9	3.27	1.6	25.4	1024	11.81	AL
24R-3, 91	187.85	1	10.7	191.3	22.9	8.49	1.9	34.7	1962	9.44	A
24R-4, 3	188.41	1	10.8	271.3	4.4	2.54	1.6	18.5	229	24.22	AL
24R-4, 17	188.55	1	9.8	275.2	9.6	1.96	0.4	27.1	164	26.11	A
24R-4, 42	188.80	1	9.2	248.6	11.2	2.22	0.9	—	183	45.00	T
24R-4, 45	188.83	1	10.4	251.7	14.7	2.33	0.8	26.9	166	51.88	AL
144-875C-											
15M-1, 11	126.71	1	10.1	—	—	0.70	—	—	1597	0.96	T
15M-1, 13	126.73	1	8.7	260.7	38.8	0.38	1.5	24.1	1349	1.05	AL
15M-1, 24	126.84	1	10.0	251.8	35.0	0.31	4.5	26.8	881	0.75	A
15M-1, 45*	127.05	1	10.8	257.4	-30.5	5.38	0.3	79.8	762	15.39	AL
15M-1, 72*	127.32	1	7.3	134.6	-21.3	4.13	3.2	—	1272	11.99	T
144-876A-											
15R-1, 28	139.68	1A	9.7	260.4	12.8	4.61	1.0	—	3273	5.20	T
16R-1, 6	147.88	1B	9.7	334.8	15.5	2.31	1.1	34.3	1530	3.29	A
16R-1, 17	147.97	1B	9.8	313.2	11.3	2.00	13.7	—	1151	3.79	T
16R-1, 21	148.03	1B	8.2	325.0	13.3	2.90	0.6	34.7	1315	8.14	AL
16R-1, 64	148.44	2	10.8	292.7	-7.1	2.61	0.4	17.4	965	5.89	AL
16R-1, 78	148.60	2	8.2	93.6	-6.0	1.69	0.5	—	954	6.56	T
17R-1, 7	150.07	2	8.2	124.1	2.5	4.29	0.9	23.1	1391	11.39	AL
17R-1, 10	150.10	2	10.2	130.4	4.1	2.61	1.0	—	1040	5.47	T
17R-1, 26	150.26	2	8.1	134.9	4.9	1.14	2.9	19.1	560	4.45	A
17R-1, 91	150.91	3	10.2	48.6	3.0	5.65	1.5	52.9	2009	6.13	A
144-877A-											
20R-1, 23*	182.93	BR	—	176.9	-34.1	0.01	3.6	3.6	—	—	A
20R-2, 72*	184.47	BR	—	174.0	16.1	0.00	2.6	—	—	—	A
20R-3, 25*	185.52	BR	—	192.0	63.1	0.00	4.6	13.3	—	—	A
20R-4, 111	183.92	1	10.4	—	—	10.45	—	13.7	2546	15.17	AL
20R-4, 115	187.92	1	19.0	180.4	8.2	10.90	1.4	11.3	7290	6.02	A
20R-4, 138	188.15	1	9.4	144.0	10.3	1.09	0.9	—	235	10.12	T
20R-5, 6	188.24	1	10.0	83.9	4.7	1.27	0.6	—	395	7.01	T
20R-5, 14	188.32	1	8.9	79.7	12.4	2.25	2.2	27.2	751	6.52	A
20R-5, 19	188.37	1	7.8	75.0	13.2	15.72	0.8	20.8	2301	25.26	AL

Notes: Abbreviations and symbols as in Table 3. BR = breccia.

COMPARISON TO SEAMOUNT MAGNETIC ANOMALY MODELING

Paleopoles derived from seamount magnetic anomalies provide a valuable source of information on the past motions of the Pacific Plate (e.g., Francheteau et al., 1970; Hildebrand and Parker, 1987). Seamount paleopoles are available for three of the guyots drilled during Leg 144. Bryan et al. (1993) reported a paleolatitude of 14°S for Lo-En Guyot based on least-squares modeling of their preferred subset of bathymetry and magnetic data. Sager et al. (1993) determined paleolatitudes for MIT and Takuyo-Daisan guyots of 32.8°S and 2.5°N, respectively. Our paleolatitude estimates for Lo-En, MIT, and Takuyo-Daisan guyots differ from those derived from seamount magnetic anomaly modeling. The normal-polarity, Southern Hemisphere magnetizations of Lo-En and Takuyo-Daisan guyots yield paleolatitudes farther south than those derived from the sea-surface anomaly data, consistent with the presence of significant viscous or induced magnetization (e.g., Gee et al., 1989). Similarly, the paleolatitude of MIT Guyot (11°S) is farther north than the paleolatitude derived from anomaly modeling (32.8°S), as expected if the magnetic anomaly of

this predominantly reversed polarity seamount includes a significant contribution from viscous/induced magnetizations. The discrepancy between the paleolatitude estimates for Takuyo-Daisan Guyot may, in part, be the result of the deviation of Hole 879A from vertical.

COMPARISON TO PREVIOUS ABSOLUTE-MOTION MODELS OF THE PACIFIC PLATE

We estimated the paleolatitudes of guyots from the age data and two previously published absolute-motion models of the Pacific Plate (Duncan and Clague, 1985; Fleitout and Moriceau, 1992). Our results are most consistent with the Pacific absolute-motion model of Duncan and Clague (1985). These authors determined the absolute motion of the Pacific Plate in the hotspot reference from using age data of seamounts and their geometry. The differences between our paleolatitudes and paleolatitude estimates of Limalok (15°S), Lo-En (25°S), MIT (14°S), and Takuyo-Daisan (7°S) guyots from the model of Duncan and Clague (1985) are smaller than 6° and are within the 95% confidence limits for our average inclinations. The paleolatitude estimate for Wodejebato Guyot (21°S) from the plate motion model

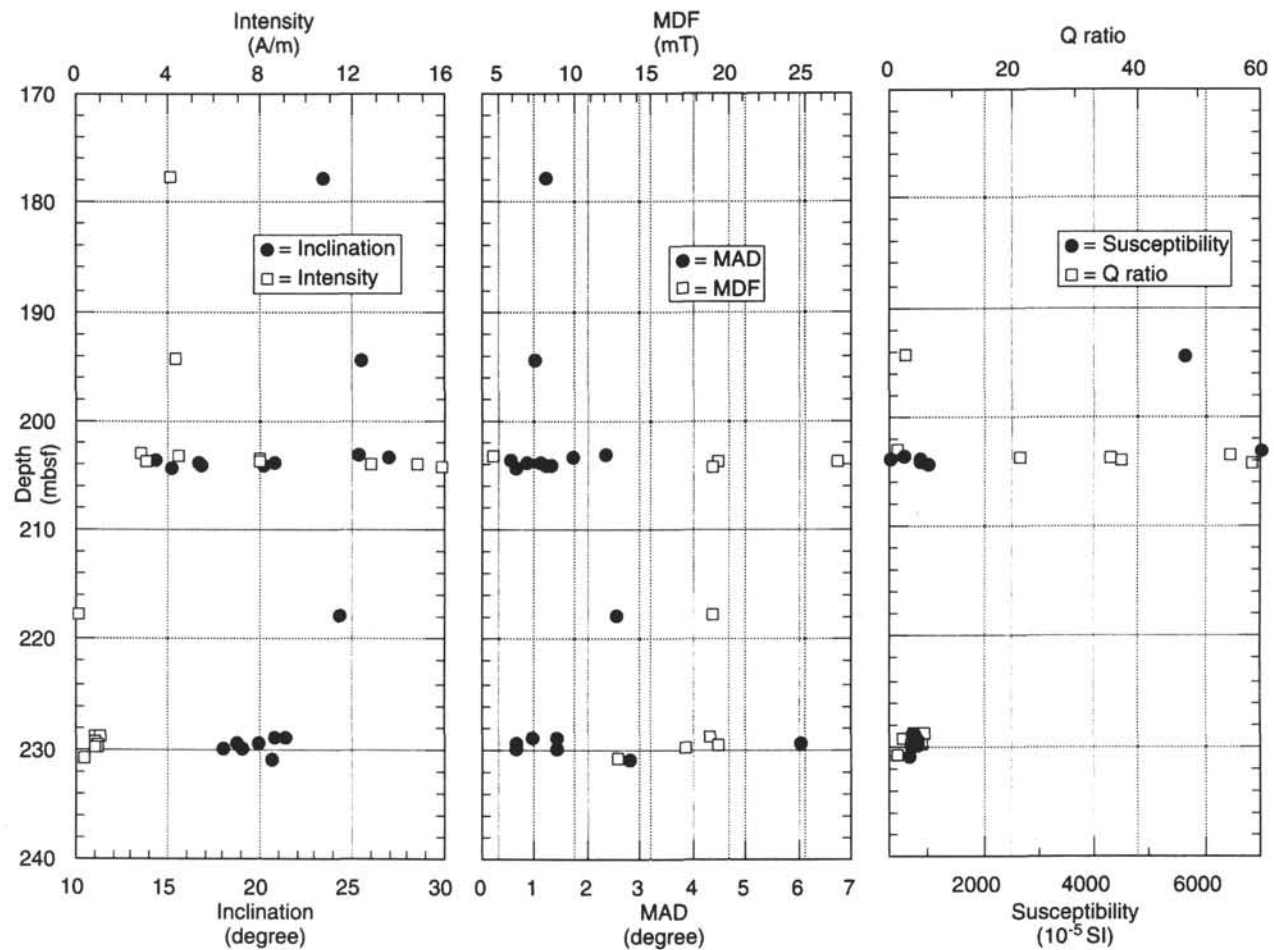


Figure 9. Paleomagnetic parameters, inclinations, NRM intensities, MADs, MDFs, susceptibilities, and Q ratios of Hole 873A vs. depth.

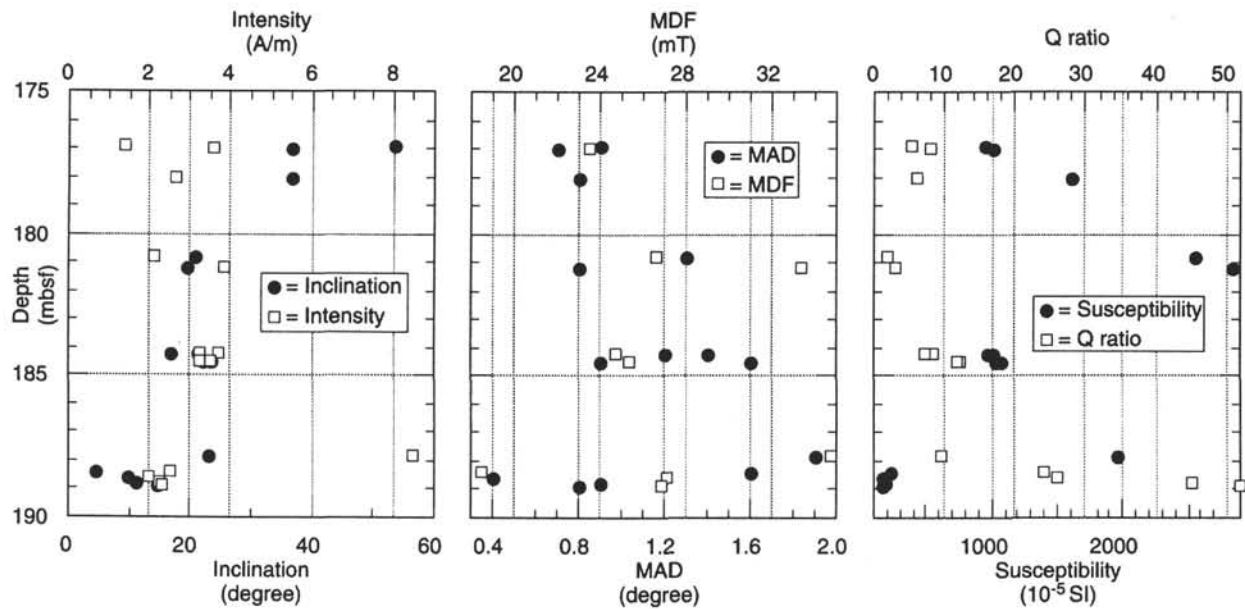


Figure 10. Paleomagnetic parameters, inclinations, NRM intensities, MADs, MDFs, susceptibilities, and Q ratios of Hole 874B vs. depth.

Table 6. AF and thermal demagnetizations of polymictic breccia from MIT Guyot.

Core, section, interval (cm)	Depth (mbsf)	Flow unit	Volume (cm ³)	Declination (degree)	Inclination (degree)	Intensity (mA/m)	MAD (degree)	MDF (mT)	Susceptibility (10 ⁻⁵ SI)	Q ratio	Demagnetization
144-878A-											
44M-1, 126	407.36	PB	9.1	—	—	30.60	0.9	39.3	18	0.10	A
44M-2, 34	407.94	PB	7.2	260.9	-33.7	30.60	—	29	2.30	—	A
45M-1, 21	409.11	PB	9.1	144.7	-31.9	35.30	2.0	39.4	34	2.26	A
45M-1, 52	409.42	PB	9.3	182.2	-33.3	40.00	2.6	45.7	40	2.89	AL
45M-1, 54	409.44	PB	7.2	184.4	-23.9	40.00	4.9	—	58	2.40	T
45M-2, 67	410.95	PB	7.8	148.2	-29.2	60.80	4.7	31.6	50	2.65	A
45M-3, 97	412.67	PB	10.1	127.3	-38.3	41.50	2.6	23.2	54	1.68	A
46M-1, 44	418.94	PB	9.8	196.9	-63.7	23.70	7.3	15.3	45	1.15	A
46M-1, 52	419.02	PB	8.9	68.2	-43.2	17.40	3.7	11.3	239	0.16	A
46M-1, 112	419.62	PB	10.4	299.8	-60.0	2212.00	3.0	3.3	3116	1.55	AL
46M-1, 126	419.76	PB	9.5	54.9	-63.7	1290.00	3.8	—	3564	0.79	T
47R-1, 104	429.24	PB	9.7	135.0	-33.4	3.00	2.0	15.7	19	0.51	AL
47R-1, 106	429.26	PB	9.7	—	—	2.00	—	—	21	0.31	T
47R-2, 27	429.97	PB	9.4	—	—	10.10	—	1.6	32	0.69	A
48R-1, 1	435.51	PB	10.0	215.3	-35.4	3.10	9.1	18.8	60	0.11	A
48R-1, 52	436.02	PB	9.2	18.9	-40.2	6.60	2.6	13.3	27	0.53	AL
49R-1, 117	446.27	PB	9.8	295.4	-28.6	7.40	4.0	8.7	56	0.29	AL
49R-2, 18	446.80	PB	8.9	275.6	-27.7	32.30	2.8	15.5	35	2.01	A
50R-2, 66	456.94	PB	8.8	208.4	-15.0	2.00	7.1	—	15	0.29	A
50R-2, 70	456.98	PB	8.0	158.0	-53.0	4.30	10.6	—	48	0.19	T
51R-1, 29	464.69	PB	9.8	357.9	-32.1	39.70	3.1	14.1	40	2.16	A
51R-2, 35	466.22	PB	11.1	157.4	-43.9	30.00	1.2	13.1	25	3.51	AL
51R-2, 38	466.25	PB	10.2	155.7	-36.7	30.00	1.6	—	29	2.94	T
51R-3, 28	467.54	PB	10.0	27.3	-41.8	50.20	1.4	21.2	40	2.74	A
51R-4, 111	469.71	PB	12.1	16.6	-52.8	2.00	5.0	—	20	0.27	T
51R-4, 114	469.74	PB	9.8	—	—	4.90	—	—	20	0.53	A
51R-5, 9	470.06	PB	9.9	174.5	-26.2	8.60	6.0	13.8	14	1.34	A
51R-6, 74	472.11	PB	9.7	225.1	-32.6	12.40	2.9	13.7	25	1.08	A
52R-1, 141	475.51	PB	9.6	125.3	-39.8	29.00	3.9	12.4	18	3.51	A
52R-2, 92	476.50	PB	9.4	298.2	-54.1	10.20	3.2	7.5	19	1.17	A
53R-1, 96	484.66	PB	8.5	114.4	-50.1	0.80	5.7	47.2	17	0.10	A
53R-2, 70	485.71	PB	9.9	44.8	-37.3	1.30	4.4	31.3	17	0.17	A
53R-2, 79	485.80	PB	9.6	135.5	-30.3	0.73	4.0	—	54	0.03	T
53R-3, 70	487.16	PB	10.5	—	—	0.05	—	—	3	0.04	A
53R-4, 49	488.40	PB	10.8	—	—	1.00	—	—	10	0.22	A
54R-1, 61	493.81	PB	7.6	137.7	-65.9	40.00	0.9	21.6	22	3.96	A
54R-2, 75	495.32	PB	8.5	139.9	-20.5	19.50	6.7	16.7	22	1.93	A
54R-3, 104	496.88	PB	8.8	224.5	-40.0	32.00	2.7	15.1	32	2.18	A
54R-6, 24	499.95	PB	8.0	262.0	-43.0	61.70	1.6	17.6	42	3.20	A
54R-6, 28	499.99	PB	9.2	—	—	31.29	—	—	87	0.79	T
55R-2, 118	504.95	PB	9.2	280.0	-41.0	41.80	0.8	15.0	30	3.04	A
55R-4, 110	507.74	PB	9.9	73.5	-18.9	43.50	3.5	14.8	27	3.51	A
55R-6, 100	510.37	PB	9.6	—	—	1.03	—	—	18	0.12	T
55R-6, 104	510.41	PB	8.5	208.3	-15.7	43.50	1.2	53.8	86	1.10	A
56R-2, 56	513.90	PB	8.9	140.4	-41.0	10.50	6.3	13.5	22	1.04	A
56R-3, 16	514.96	PB	11.1	0.5	-51.7	10.00	2.3	—	44	0.71	AL
56R-3, 20	518.96	PB	8.2	—	—	20.00	—	—	79	0.83	T
56R-3, 78	515.58	PB	10.2	32.6	-36.0	23.00	2.4	11.4	51	0.98	A
56R-6, 28	519.20	PB	9.6	124.4	-41.4	46.10	1.4	12.4	55	1.83	A
57R-1, 37	521.57	PB	9.5	35.2	-46.5	58.50	2.8	14.2	73	1.75	A
57R-3, 60	524.39	PB	9.7	306.5	-44.9	33.80	1.6	—	99	0.74	T
57R-3, 63	524.42	PB	9.8	214.5	-40.8	40.00	2.5	14.4	64	1.36	A
57R-5, 102	527.71	PB	10.0	211.5	-36.4	74.40	1.3	14.7	102	1.59	A
58R-2, 105	532.95	PB	12.1	123.4	-38.1	80.00	0.7	15.1	93	2.90	AL
58R-2, 107	532.97	PB	12.6	130.1	-36.7	70.00	2.4	—	88	2.61	T
58R-3, 96	534.30	PB	9.3	24.4	-36.8	60.70	0.8	15.3	90	1.47	A
58R-5, 53	536.48	PB	9.8	166.2	-47.0	80.80	2.4	15.9	113	1.56	A
58R-7, 88	539.35	PB	9.7	254.5	-44.9	107.10	2.3	13.8	104	2.25	A
59R-1, 23	540.33	PB	0.0	—	—	—	—	—	—	—	T
59R-3, 40	543.04	PB	8.9	152.6	-45.2	71.90	3.6	14.3	93	1.69	A
59R-4, 76	544.86	PB	8.2	68.6	-43.4	67.90	2.4	14.1	105	1.41	A
59R-5, 37	545.67	PB	9.3	271.0	-44.4	31.20	4.3	15.9	64	1.06	A
59R-6, 21	546.55	PB	9.7	98.8	-52.2	50.00	1.4	16.8	88	1.90	AL
59R-6, 24	546.58	PB	10.7	91.6	-57.1	50.00	4.3	—	105	1.66	T
59R-7, 38	548.13	PB	9.6	11.7	-39.7	98.40	1.1	15.2	122	1.76	A
60R-2, 60	551.77	PB	9.6	335.9	-59.9	43.90	2.8	16.1	60	1.60	A
60R-3, 101	553.62	PB	9.5	—	—	17.80	—	—	130	0.30	T
60R-3, 106	553.67	PB	9.1	234.3	-41.3	26.80	1.8	22.3	81	0.72	A
60R-5, 22	555.26	PB	10.4	227.9	-35.2	61.90	1.6	15.1	106	1.27	A
60R-6, 27	556.83	PB	8.4	32.8	-42.2	46.40	1.2	19.4	62	1.63	A
61R-2, 13	560.84	PB	9.8	39.5	-28.7	100.20	8.2	25.5	230	0.95	A
61R-3, 85	563.06	PB	11.6	40.6	-66.3	30.00	1.2	—	65	1.72	T
61R-3, 89	563.10	PB	11.1	39.1	-36.4	40.00	1.7	13.6	73	1.88	AL
61R-4, 96	564.63	PB	10.0	183.7	-36.3	18.90	3.7	13.1	22	1.87	A
61R-5, 78	565.91	PB	10.3	156.0	-43.0	16.40	1.5	12.2	53	0.67	AL
62R-2, 78	570.59	PB	9.3	204.6	-62.8	1.30	6.8	36.1	15	0.19	A
62R-3, 124	572.56	PB	9.6	180.5	-48.6	46.00	5.9	14.2	114	0.88	AL
62R-4, 46	573.26	PB	10.1	251.5	-45.8	48.40	3.7	17.9	85	1.24	A
62R-6, 107	576.66	PB	9.7	224.7	-35.3	30.00	4.2	—	73	1.45	T
62R-6, 110	576.69	PB	10.2	186.1	-32.4	30.00	1.0	15.6	59	1.66	AL
63R-1, 77	578.87	PB	9.6	292.9	-27.1	23.10	3.1	12.5	29	1.74	A
63R-3, 48	581.57	PB	9.7	258.0	-45.6	10.00	5.5	—	21	2.03	T
63R-3, 52	581.61	PB	9.7	—	—	10.00	—	14.9	60	0.80	AL
63R-5, 91	584.82	PB	10.3	184.6	-41.9	11.30	2.5	9.6	53	0.46	AL
63R-6, 37	585.36	PB	9.6	253.9	-24.5	20.50	4.3	12.9	29	1.54	A
64R-1, 13	587.73	PB	8.2	19.1	-24.3	25.30	0.8	14.1	39	1.41	A
64R-3, 84	591.44	PB	10.8	45.8	-40.5	17.80	2.5	9.5	127	0.31	AL
64R-5, 77	594.24	PB	9.5	182.4	-55.6	23.80	4.2	14.4	26	2.00	A
64R-7, 5	596.29	PB	10.7	51.7	-27.6	10.00	1.0	11.2	25	0.89	AL
64R-7, 14	596.38	PB	10.7	49.7	-30.1	20.00	2.6	—	30	1.70	T
65R-3, 70	600.78	PB	9.3	147.8	-27.5	20.20	2.9	12.6	24	1.84	A
65R-3, 80	600.88	PB	9.6	—	—	14.80	—	—	69	0.47	T
65R-5, 23	602.81	PB	9.6	222.3	-16.3	4.20	5.1	37.5	12	0.76	A
65R-5, 104	603.62	PB	11.1	88.5	-0.4	1.00	21.0	—	10	0.16	T
65R-5, 110	603.68	PB	11.6	—	—	0.70	—	—	9	0.26	A

Notes: Abbreviations and symbols as in Table 3. PB = polymictic breccia.

Table 7. AF and thermal demagnetizations of volcanic basement from MIT Guyot.

Core, section, interval (cm)	Depth (mbsf)	Flow unit	Volume (cm ³)	Declination (degree)	Inclination (degree)	Intensity (A/m)	MAD (degree)	MDF (mT)	Susceptibility (10 ⁻⁵ SI)	Q ratio	Demagnetization
144-878A-											
78R-2, 51	723.99	1	9.7	116.4	-18.1	5.20	1.5	3207	5.27	T	
78R-2, 57	724.05	1	8.5	106.5	-16.7	4.98	1.4	3229	5.01	AL	
78R-2, 71	724.19	1	8.3	100.2	-18.5	4.07	1.2	3415	2.60	A	
78R-2, 74	724.22	1	9.0	102.2	-17.8	3.56	2.0	4212	1.84	T	
79R-1, 107	732.77	2	8.0	230.8	-23.8	2.67	2.3	4253	1.37	AL	
79R-2, 4	733.17	2	7.3	45.7	-21.6	2.40	1.2	4857	1.61	T	
79R-2, 8	733.21	2	9.2	42.5	-21.8	2.32	1.5	4015	1.88	AL	
79R-3, 55	735.05	2	10.0	315.1	-19.5	2.18	2.4	5.1	4527	1.05	AL
80R-3, 28	744.68	8	8.5	105.1	-13.2	3.41	1.2	25.2	3232	2.30	A
80R-3, 40	744.80	8	9.2	98.2	-18.5	2.55	1.9	4283	1.94	T	
80R-5, 21	747.17	8	7.3	67.1	-20.7	6.29	1.2	1553	13.16	T	
80R-5, 26	747.22	8	7.4	56.1	-12.6	6.52	1.7	1538	9.24	A	
80R-6, 67	748.93	8	9.5	—	—	5.58	—	1407	8.65	T	
80R-6, 72	748.98	8	9.5	340.2	-23.1	11.08	0.9	5.6	1184	20.40	AL
81R-1, 15	751.15	10	9.5	256.6	-14.8	5.80	2.8	6.6	3232	3.91	A
81R-1, 19	751.19	10	9.6	248.7	-25.3	5.19	3.1	1538	7.36	T	
81R-2, 78	753.23	10	9.3	331.4	-12.7	4.81	0.8	8.1	3157	3.32	AL
81R-3, 30	753.95	10	8.7	76.2	-11.5	5.35	0.7	2466	7.05	T	
81R-3, 35	754.00	10	10.5	89.9	-14.0	6.31	2.6	7.4	3243	4.24	A
81R-4, 53	755.68	11	6.8	88.6	-12.4	12.48	0.5	3345	12.13	T	
81R-4, 58	755.73	11	9.8	94.0	-11.9	4.52	1.4	52.8	1019	9.67	A
81R-5, 11	756.63	11	9.4	5.5	-15.7	5.07	1.4	18.7	2627	4.21	AL
81R-5, 79	757.31	11	8.2	330.1	-15.3	4.97	3.2	3102	3.49	T	
81R-5, 84	757.36	11	9.5	341.1	-11.5	5.15	0.6	35.7	3522	3.19	A
82R-2, 81	762.85	12	10.6	173.9	-14.4	7.10	0.3	43.2	4068	3.81	A
82R-2, 84	762.88	12	9.3	173.9	-13.8	6.69	1.4	41.3	2891	5.04	AL
83R-3, 67	773.83	13	8.5	347.9	-37.7	1.86	1.4	14.2	1159	3.50	A
83R-4, 7	774.59	13	10.2	222.3	-24.1	3.53	0.9	6511	7.64	T	
83R-4, 11	774.63	13	8.7	215.8	-27.9	3.22	3.1	15.2	7091	4.75	AL
84R-1, 8	779.98	14	8.2	137.2	-41.7	8.07	0.9	3520	5.00	T	
84R-1, 13	780.03	14	11.0	136.9	-41.5	10.47	1.2	25.1	3289	6.94	A
84R-3, 106	783.92	15	8.6	283.5	-34.8	3.66	0.7	25.2	1372	5.82	AL
84R-4, 63	784.94	15	9.5	288.1	-23.5	3.44	0.6	1822	6.13	T	
84R-4, 67	784.98	15	8.5	288.5	-27.9	3.82	0.9	27.8	1739	7.13	AL
84R-5, 87	786.68	15	10.4	217.1	-21.6	3.03	2.0	12.2	1793	3.68	A
84R-5, 109	786.90	15	10.3	347.3	-19.8	4.06	1.8	27.1	1918	4.61	AL
84R-6, 70	787.93	15	9.6	170.6	-22.4	6.82	1.5	39.1	2575	5.77	A
84R-6, 76	787.99	15	8.7	169.5	-20.2	6.42	0.3	2702	7.73	T	
85R-1, 31	789.61	16	9.8	156.7	-15.1	12.70	1.2	26.0	3640	7.61	AL
85R-1, 142	790.72	16	8.2	293.0	-28.5	2.81	2.1	3719	2.46	T	
85R-1, 146	790.76	16	8.7	294.4	-29.9	2.74	1.1	6.9	3856	2.31	AL
85R-2, 82	791.62	16	7.9	263.7	-19.0	5.91	1.7	2429	5.30	T	
85R-2, 90	791.70	16	9.2	272.9	-23.1	6.96	3.8	19.9	2202	6.89	A
86R-3, 39	801.65	18	9.7	92.2	-24.7	1.40	0.8	947	4.80	T	
86R-3, 43	801.69	18	9.6	96.8	27.0	1.60	1.5	55.0	1027	3.40	A
88R-3, 4	820.75	20	9.9	344.7	-16.2	1.77	2.5	28.4	2899	1.33	A
88R-3, 64	821.35	20	8.7	284.4	-14.5	1.67	0.8	3392	1.60	T	
88R-3, 66	821.37	20	7.8	284.1	-7.8	2.30	2.0	34.8	3147	2.37	AL
89R-1, 49	828.09	21	78.4	299.1	-10.4	1.91	1.6	35.3	282	14.72	AL
89R-1, 52	828.12	21	8.1	302.6	-5.2	2.60	1.6	2946	1.92	T	
89R-3, 75	830.96	21	8.7	216.3	-6.8	0.84	1.5	4927	0.55	T	
89R-4, 25	831.77	21	9.0	318.3	-4.7	1.81	0.4	2399	2.45	T	
89R-4, 45*	831.97	21	10.0	134.3	-20.0	1.36	9.1	4.8	2202	1.34	A
90R-1, 15	837.35	21	7.7	50.3	-4.7	0.64	4.0	4.6	6615	0.21	AL
90R-1, 99	838.19	21	7.3	191.4	0.6	0.71	0.6	2433	0.95	T	
90R-1, 105	838.25	21	10.5	203.4	1.3	0.69	1.6	50.2	2899	0.52	A
90R-2, 36	838.82	21	10.2	286.0	-2.8	0.37	3.3	57.0	669	1.81	AL
90R-2, 40	838.86	21	7.3	282.0	-0.7	0.49	1.0	1500	1.06	T	
90R-4, 46	838.92	22	9.5	170.9	35.7	1.56	1.0	738	4.61	T	
90R-4, 70	842.16	22	9.6	212.6	35.9	0.09	0.3	—	886	0.21	AL
90R-4, 107	842.53	22	10.2	114.1	35.0	0.83	1.1	—	439	6.12	AL
90R-4, 115	842.61	22	7.3	110.0	36.2	1.19	0.7	574	6.75	T	
90R-5, 94	843.90	23	7.3	111.0	28.4	1.95	0.5	619	10.21	T	
90R-5, 98	843.94	23	11.1	110.4	31.3	1.55	1.8	25.3	754	6.68	AL
90R-6, 3	844.39	23	10.7	265.3	33.2	0.33	2.9	15.5	5739	0.12	AL
90R-6, 49*	844.85	23	9.1	—	—	0.63	—	5064	0.27	T	
91R-1, 97	847.47	23	9.2	229.1	30.8	0.30	1.9	2929	0.33	T	
91R-1, 103	847.53	23	10.4	234.6	39.5	0.41	2.3	—	1837	0.49	A
91R-3, 83	850.27	23	10.2	92.6	31.1	0.38	2.7	10.1	3019	0.41	AL
91R-3, 86*	850.30	23	9.2	97.3	-0.8	0.34	9.2	2690	0.41	T	
91R-4, 138	852.32	23	9.8	9.0	30.1	0.68	3.9	2.9	2604	0.57	AL
92R-1, 83	857.03	24	10.4	210.5	12.5	0.62	12.1	1583	0.85	T	
92R-1, 86	857.06	24	10.8	216.4	15.7	0.66	1.4	18.1	1550	0.93	AL
92R-1, 101	857.21	24	10.3	216.4	16.7	1.07	0.6	54.0	1777	1.31	A
92R-2, 4	857.61	25	10.4	240.6	-1.1	4.66	1.5	24.8	1602	6.35	A
92R-2, 73	858.30	25	7.3	93.7	16.5	6.39	0.8	38.8	1242	16.73	AL
92R-2, 94	858.51	25	8.7	258.3	15.8	7.68	0.5	1678	14.87	T	
92R-3, 113	860.03	26	8.2	195.1	10.6	0.74	1.2	2403	1.00	T	
92R-3, 116	860.06	26	10.4	203.9	10.8	0.43	2.2	29.0	2181	0.65	AL
92R-4, 4	860.16	26	10.3	40.3	13.1	0.25	2.3	32.3	1598	0.34	AL
92R-4, 83	860.95	26	11.6	190.0	14.1	1.09	0.9	25.1	3253	0.73	A
92R-4, 91	861.03	26	5.1	188.1	11.7	1.78	3.4	3138	1.24	T	
92R-5, 12	861.73	27	8.0	—	—	0.25	—	2084	0.27	T	
92R-5, 21	861.82	27	10.3	54.3	14.8	0.33	1.5	33.2	986	0.73	AL
92R-5, 36	861.97	27	9.2	59.4	10.6	0.54	0.7	1061	1.66	T	
93R-1, 15	865.85	28	8.2	229.3	21.3	5.54	0.5	29.7	1700	7.11	A
93R-1, 21	865.91	28	8.7	224.2	22.5	1.65	1.3	2967	1.81	T	
93R-1, 55	866.25	28	8.0	227.2	21.4	4.24	1.0	1441	6.42	T	
93R-1, 59	866.29	28	8.6	225.3	22.1	2.80	0.6	49.1	1085	5.63	AL
93R-2, 22	867.41	29	10.6	176.3	20.5	0.57	1.7	28.2	1683	0.74	AL
93R-2, 123	868.42	30	7.4	17.9	20.9	5.99	0.4	34.9	848	15.41	A
93R-2, 129	868.48	30	9.5	8.9	15.4	4.82	1.0	1418	7.41	T	
93R-3, 86	869.49	30	11.0	177.2	18.7	2.80	1.7	41.7	574	10.64	AL
94R-1, 9	875.49	30	8.2	157.5	7.2	1.42	1.4	5081	0.91	T	
95R-2, 18	886.29	31B	9.7	353.8	22.7	4.21	0.7	47.9	508	26.96	AL
95R-2, 20	886.31	31B	10.2	0.3	26.3	3.54	0.8	413	27.80	T	
95R-5, 114	891.36	32	9.5	54.6	21.5	10.93	1.0	37.2	3090	7.71	AL
95R-6, 2	891.68	32	10.8	96.9	20.3	0.64	3.2	67.7	848	1.64	A
95R-6, 10	891.76	32	9.5	92.0	14.7	2.45	2.4	3131	1.71	T	

Table 7 (continued).

Core, section, interval (cm)	Depth (mbsf)	Flow unit	Volume (cm ³)	Declination (degree)	Inclination (degree)	Intensity (A/m)	MAD (degree)	MDF (mT)	Susceptibility (10 ⁻⁵ SI)	Q ratio	Demagnetization
97R-1, 113	895.53	34	7.3	156.5	28.8	0.36	2.5	—	2260	0.51	AL
97R-2, 124	897.14	34	9.7	—	—	0.38	—	1908	0.44	T	
97R-2, 128	897.18	34	9.9	86.4	19.4	0.68	1.2	15.4	2607	0.57	A
98R-2, 98	906.33	35	10.6	46.1	35.8	0.26	2.6	44.3	1424	0.39	AL
98R-3, 46	907.25	35	12.4	160.0	35.6	2.05	4.0	2.3	1839	2.43	A
98R-3, 58	907.37	35	7.8	—	—	0.91	—	—	1309	1.51	T
98R-3, 88	907.67	35	8.7	255.4	32.2	1.36	0.7	19.2	725	6.08	AL
98R-3, 96	915.67	35	11.1	—	—	1.12	—	1526	2.38	T	

Notes: Abbreviations and symbols as in Table 3.

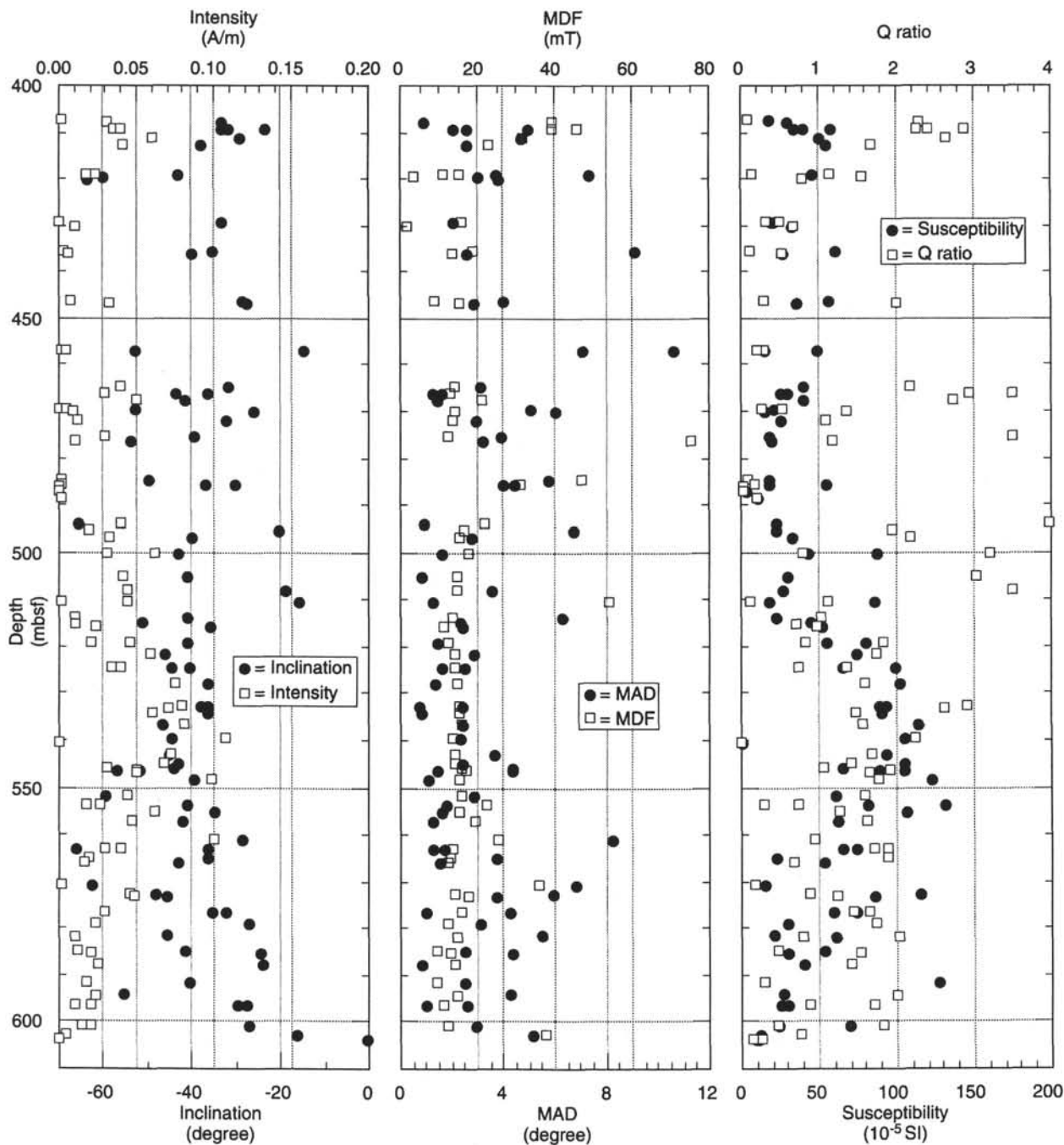


Figure 11. Paleomagnetic parameters, inclinations, NRM intensities, MADs, MDFs, susceptibilities, and Q ratios of polymictic breccia in Hole 878A vs. depth.

Table 8. AF and thermal demagnetizations from Takuyo-Daisan Guyot.

Core, section, interval (cm)	Depth (mbsf)	Flow unit	Volume (cm ³)	Declination (degree)	Inclination (degree)	Intensity (A/m)	MAD (degree)	MDF (mT)	Susceptibility (10 ⁻⁵ SI)	Q ratio	Demagnetization
144-879A-											
22R-1, 73	198.83	I	8.9	148.9	-11.4	1.32	7.1	21.1	437	6.60	A
22R-2, 91	200.38	I	10.8	62.9	-17.3	10.28	1.9	42.5	567	39.53	A
22R-2, 116	200.63	I	9.7	256.5	-26.9	4.28	1.0		434	21.49	T
22R-2, 126	200.73	I	10.4	242.1	-28.1	4.37	1.6	24.2	396	24.05	AL
22R-3, 129	202.26	I	9.2	340.9	-10.8	2.07	0.9	22.1	354	16.70	AL
22R-3, 136	209.26	I	10.2	338.4	-2.2	2.35	0.7		367	18.31	T
22R-5, 44	204.25	I	10.5	185.8	-8.0	4.73	0.9	58.7	244	42.23	A
22R-5, 67	204.48	I	9.7	181.8	-25.3	4.01	1.0		251	45.63	T
22R-5, 74	204.55	I	10.2	179.0	-23.4	4.33	1.4	29.1	442	28.02	AL
22R-7, 38	206.93	I	10.7	83.0	-18.1	2.93	0.5	50.6	154	41.50	AL
23R-1, 105	208.65	I	8.2	332.9	-37.8	0.15	4.3	20.4	462	0.93	AL
23R-1, 108	208.68	I	8.7	326.7	-15.3	0.20	6.5		202	2.79	T
23R-5, 34	213.87	I	9.5	117.5	-15.8	3.49	2.2		562	13.55	T
23R-5, 37	213.90	I	10.9	118.5	-15.4	3.70	1.1	15.5	579	13.93	AL

Notes: Abbreviations and symbols as in Table 3.

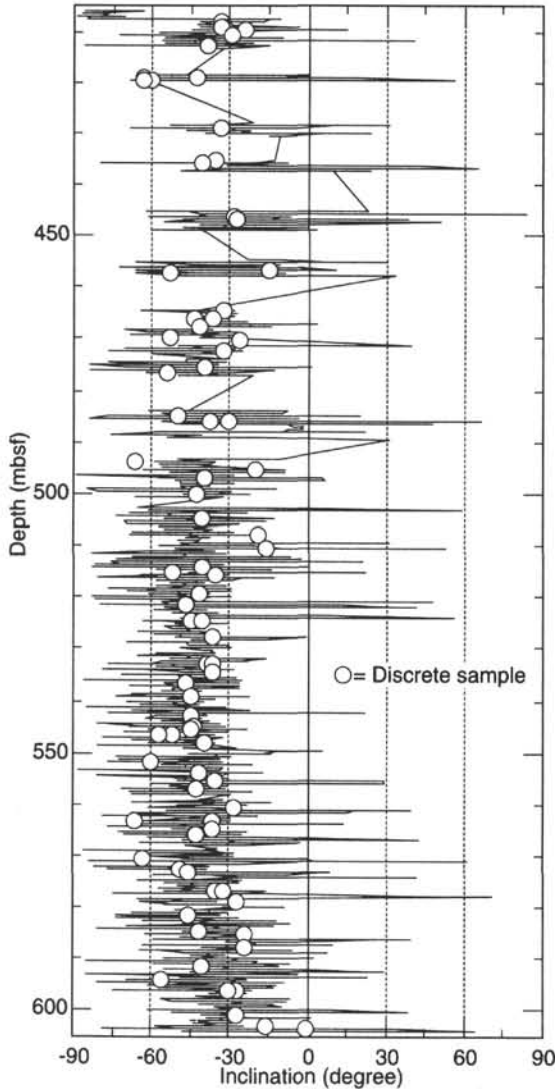


Figure 12. Results of the shipboard whole-core measurements of the polymictic breccia from MIT Guyot (Site 878) after AF demagnetization at 15 mT as well as those of discrete samples.

of Duncan and Clague (1985), however, is considerably different than that derived from samples recovered during Leg 144. Winterer et al. (1993) have suggested that the French Polynesian hotspots have drifted $\sim 10^\circ\text{--}12^\circ$ south with respect to the paleomagnetic reference frame, similar to the southward drift suggested in previous studies (e.g., Gordon and Cape, 1981; Sager and Bleil, 1987). The difference

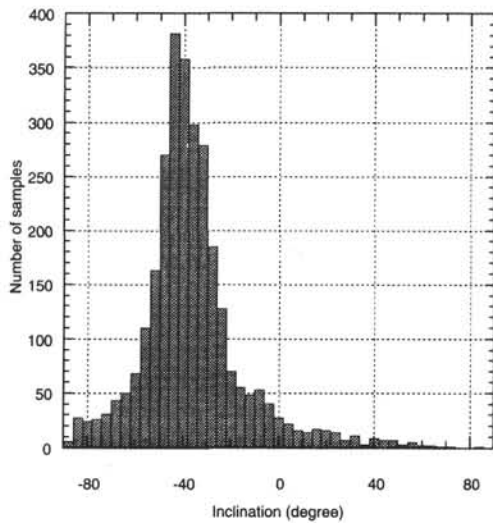


Figure 13. Histogram of archive half-core inclinations from polymictic breccia of MIT Guyot (Site 878).

between our paleolatitudes and those from Duncan and Clague (1985) except for Wodejebato Guyot is smaller ($<6^\circ$).

COMPARISON TO THE PACIFIC APPARENT POLAR WANDER PATH

Larson and Sager (1992) constructed an apparent polar wander path (APWP) for the Pacific Plate based on seamount paleopoles from 39 to 88 Ma and on crustal magnetic lineations from 122 to 155 Ma. Two separate paths were calculated for the older portion of the APWP, with anomalous skewness and without anomalous skewness. Figure 20 illustrates the paleocolatitudes of guyots from Leg 144 as well as the APWP without anomalous skewness (Larson and Sager, 1992). The paleocolatitudes of Takuyo-Daisan and Lo-En guyots do not intersect with the APWP. The intersections of the small circles for Limalok, Wodejebato, and MIT guyots with the APWP suggest ages of about 50, 70, and 123 Ma (or 134 Ma), respectively. The ages of the Limalok and Wodejebato guyots, as suggested by their intersections with the APWP, are younger than those proposed by the results of Leg 144. The age of MIT Guyot determined from the APWP without anomalous skewness is similar to that of the radiometric age determined by Pringle et al. (this volume), although the age from the APWP without anomalous skewness is different.

SUMMARY

We conducted paleomagnetic studies of 340 discrete samples of volcanic rocks collected during Leg 144. Stepwise thermal and AF

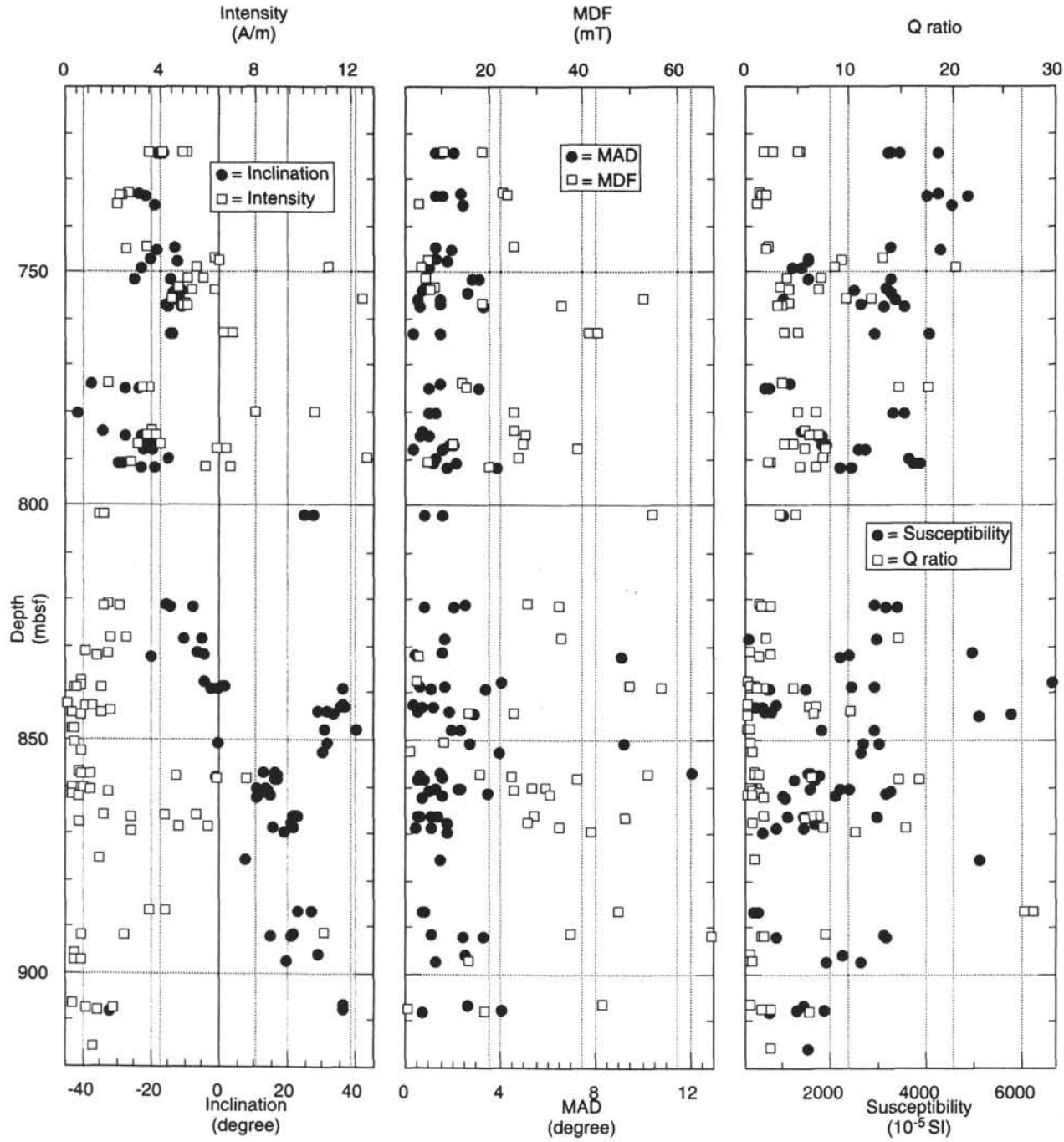


Figure 14. Paleomagnetic parameters, inclinations, NRM intensities, MADs, MDFs, susceptibilities, and Q ratios of samples from the volcanic basement in Hole 878A vs. depth.

demagnetizations typically isolate the same characteristic magnetization direction. The moderate MDFs and Q ratios and the lack of significant low-stability magnetizations in most samples suggest that the magnetization of these samples is relatively stable. In most cases, the observed scatter in inclination values compares favorably with that predicted from models of paleosecular variation. The presence of both normal and reversed polarity lavas from MIT Guyot and the consistency of results from five sites on the summit of Wodejebato Guyot suggest that the paleolatitudinal estimates for these guyots are particularly robust. The radiometric age of volcanic rocks from MIT Guyot (122.9 ± 0.9 Ma; Pringle et al., this volume) implies that the reversed polarity corresponds to Chron M1 or older. Radiometric age determinations for Wodejebato Guyot range from 79 to 85 Ma

(Pringle et al., this volume), compatible with a reversed polarity remanence acquired during Chron C33R.

Paleolatitudes from the combined shipboard and shore-based paleomagnetic data are about 10° S, except for Lo-En Guyot, which has a paleolatitude of about 31° S. We also estimated paleolatitudes of guyots from the age data and from a previously published absolute plate-motion model for the Pacific Plate. Differences between these paleolatitude estimates and those derived from remanence measurements are smaller than 6° . Our paleolatitude estimates for Lo-En, MIT, and Takuyo-Daisan guyots differ from those derived from previous seamount magnetic-anomaly modeling. The sense and magnitude of this discrepancy are compatible with a significant contribution from viscous and induced magnetizations.

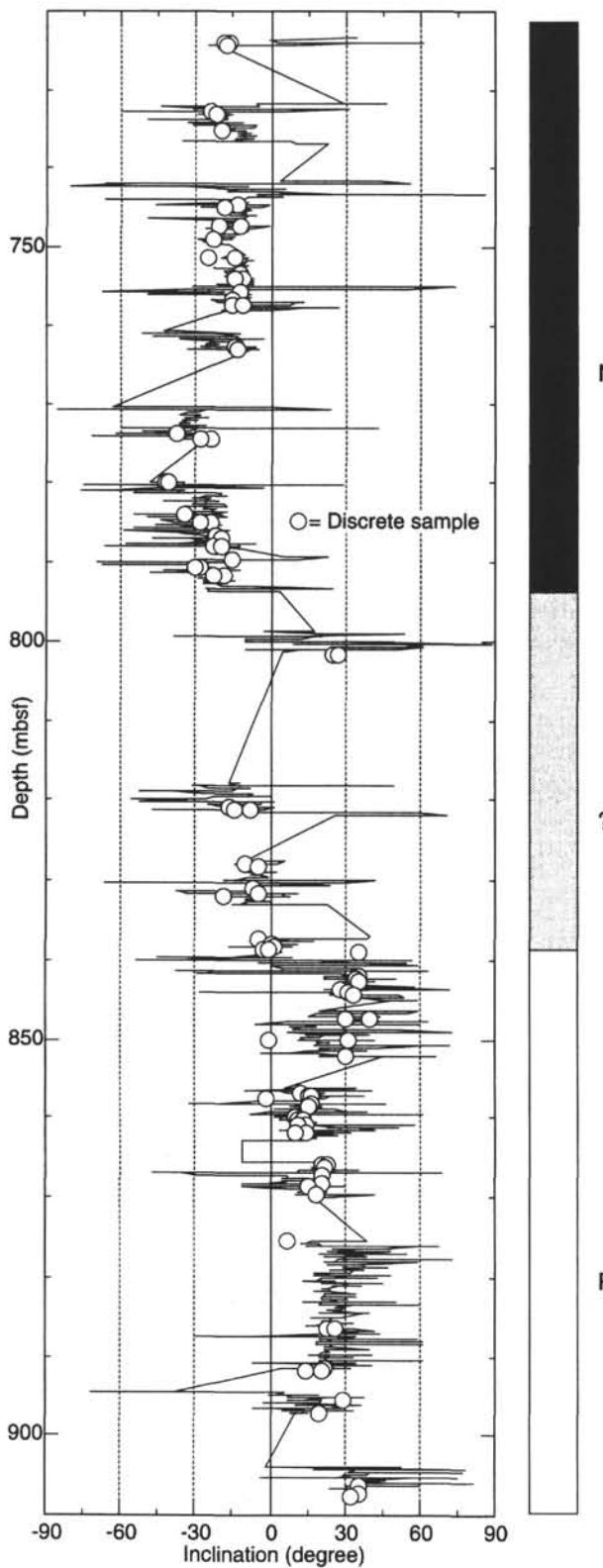


Figure 15. Discrete sample and shipboard archive half-core remanence data (after 15 mT) from the volcanic basement at MIT Guyot (Site 878).

Table 9. Average inclinations for each flow unit.

Flow unit	<i>N</i>	Average inclination	α	<i>k</i>
Hole 871C:				
1	5	-5.3	9.8	93.6
7A	1	-32.6		
9	4	-31.2	6.1	380.0
10	1	-33.3		
13	5	-16.4	6.0	225.0
15	6	-9.0	4.4	289.0
16	1	-8.0		
17	5	-18.6	7.0	162.0
19	5	-19.6	5.4	276.0
21	5	-19.1	4.4	419.0
22	5	-15.7	4.8	344.0
23	1	-17.9		
Hole 872A:				
1	2	-32.7		
Hole 872B:				
6	4	-47.4	4.2	931.0
9	4	-49.1	9.3	165.0
10B	4	-49.4	2.3	2792.0
13	4	-44.9	2.2	2857.0
14	4	-54.4	8.2	211.0
15B	4	-52.3	6.1	379.0
16	6	-48.1	7.3	104.0
17	4	-60.0	1.6	3142.0
18B	4	-49.6	23.6	23.4
1	4	-45.7	13.2	93.1
Hole 873A:				
4	1	23.4		
7	1	25.5		
8	8	19.6	4.7	151.0
9	8	20.3	2.0	869.0
Hole 874B:				
1A	7	20.9	2.5	654.0
1B	4	10.0	9.0	179.0
Hole 875C:				
1	3	34.8	14.9	190.0
Hole 876A:				
1	4	13.2	3.6	1086.0
2	5	-0.3	9.0	98.8
3	1	3.0		
Hole 877A:				
1	6	8.4	5.9	160.0
Hole 878A:				
PB	64	-38.20	32.43	0.7
1	4	-17.8	1.6	5509.0
2	4	-21.7	3.7	1063.0
8	5	-17.7	7.2	155.0
10	5	-15.7	8.7	107.0
11	5	-13.4	3.1	834.0
12	2	-14.1		
13	3	-30.1	25.4	66.7
14	2	-41.6		
15	7	-24.4	6.0	115.0
16	5	-23.2	9.8	84.1
18	2	25.9		
20	3	-12.9	16.0	167.0
21	9	-2.7	4.3	153.0
22	4	35.7	1.1	12633.0
23	7	32.1	4.0	256.0
24	3	15.0	7.9	682.0
25	2	16.2		
26	5	12.1	2.4	1444.0
27	2	12.7		
28	4	21.8	1.2	9971.0
29	1	20.5		
30	4	15.6	12.6	91.1
31	2	24.5		
32	3	18.9	13.0	249.0
34	2	24.2		
35	3	34.5	7.3	802.0
Hole 879A:				
1	14	-19.2	6.0	42.0

Notes: PB = polymictic breccia of Hole 878A. *N* = number of flow units.

Table 10. Average inclinations of guyots.

Guyot	<i>N</i>	Average inclination	α	<i>k</i>	Paleo-latitude	Predicted <i>k</i>	Present latitude
Limalok	12	-19.0	7.1	37.5	-9.8	26.9	5.6°N
Lo-En	11	-49.8	5.4	72.6	-30.6	39.4	10.1°N
Wodejebato	11	16.5	8.3	30.3	-8.4	26.4	11.9°N
MIT	23	-22.1	4.1	50.1	-11.4	27.5	27.3°N
Takuyo-Daisan	1	-19.2	6.0	42.6	-9.9	26.9	34.2°N

Note: *N* = number of flow units.

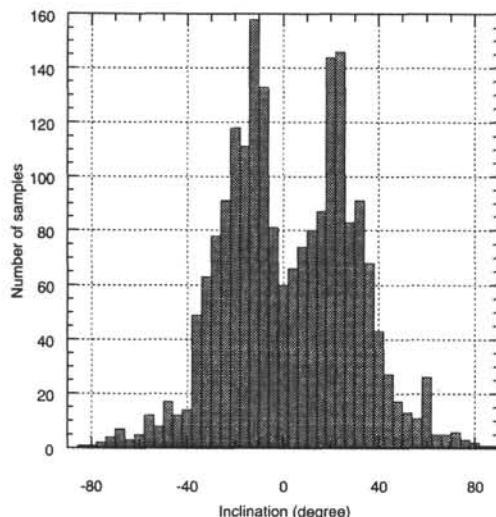


Figure 16. Histogram of inclinations of the volcanic basement from MIT Guyot (Site 878) by whole-core measurements.

ACKNOWLEDGMENTS

We are grateful to ODP for enabling us to participate during Leg 144. This study was supported by the Japan Ocean Drilling Program (M.N.). M. Nakanishi thanks Professor A. Taira and the Japan ODP Office for efforts regarding his participation in Leg 144. This research was supported in part by USSAC Grant No. J44-20747 to J. Gee. We thank Dr. Kazuo Kobayashi for his critical comments. We appreciate the helpful reviews by Drs. M. McNutt, M. Torii, and H. Inokuchi.

REFERENCES*

- Bryan, P.C., Shoberg, T., Gordon, R.G., Petronotis, K.E., and Bergersen, D.D., 1993. A paleomagnetic pole and estimated age for Lo-En Guyot, Republic of the Marshall Islands. *In* Pringle, M.S., Sager, W.W., Sliter, W.V., and Stein, S. (Eds.), *The Mesozoic Pacific: Geology, Tectonics, and Volcanism*. Geophys. Monogr., Am. Geophys. Union, 77:387–400.
- Butler, R.F., 1992. *Paleomagnetism: Magnetic Domains to Geologic Terranes*. Boston (Blackwell).
- Duncan, R.A., and Clague, D.A., 1985. Pacific plate motion recorded by linear volcanic chains. *In* Nairn, A.E.M., Stehli, F.G., and Uyeda, S. (Eds.), *The Ocean Basins and Margins* (Vol. 7A): *The Pacific Ocean*. New York (Plenum), 89–121.
- Fleitout, L., and Moriceau, C., 1992. Short-wavelength geoid, bathymetry and the convective pattern beneath the Pacific Ocean. *Geophys. J. Int.*, 110:6–28.
- Francheteau, J., Harrison, C.G.A., Sclater, J.G., and Richards, M.L., 1970. Magnetization of Pacific seamounts: a preliminary polar curve for the northeastern Pacific. *J. Geophys. Res.*, 75:2035–2061.
- Fukao, Y., 1992. Seismic tomogram of the Earth's mantle: geodynamics implications. *Science*, 258:625–630.
- Gee, J., Staudigel, H., and Tauxe, L., 1989. Contribution of induced magnetization to magnetization of seamounts. *Nature*, 342:170–173.
- Hess, H.H., 1946. Drowned ancient islands of the Pacific basin. *Am. J. Sci.*, 244:772–791.
- Hildebrand, J.A., and Parker, R.L., 1987. Paleomagnetism of Cretaceous Pacific seamounts revisited. *J. Geophys. Res.*, 92:12695–12712.
- Irving, E., and Pullaiah, G., 1976. Reversal of the geomagnetic field, magnetostratigraphy and relative magnitude of palaeosecular variation in the Phanerozoic. *Earth-Sci. Rev.*, 12:35–64.
- Kirschvink, J.L., 1980. The least-squares line and plane and analysis of palaeomagnetic data. *Geophys. J. R. Astron. Soc.*, 62:699–718.
- Kono, M., 1980. Paleomagnetism of DSDP Leg 55 basalts and implications for the tectonics of the Pacific plate. *In* Jackson, E.D., Koizumi, I., et al., *Init. Reps. DSDP*, 55: Washington (U.S. Govt. Printing Office), 737–752.
- Larson, R.L., 1991. The latest pulse of the Earth: evidence for a mid-Cretaceous super plume. *Geology*, 19:547–550.
- Larson, R.L., and Sager, W.W., 1992. Skewness of magnetic anomalies M0 to M29 in the northwestern Pacific. *In* Larson, R.L., Lancelot, Y., et al., *Proc. ODP, Sci. Results*, 129: College Station, TX (Ocean Drilling Program), 471–481.
- McFadden, P.L., 1980. Testing a paleomagnetic study for the averaging of secular variation. *Geophys. J. R. Astron. Soc.*, 61:183–192.
- McFadden, P.L., Merrill, R.T., and McElhinny, M.W., 1988. Dipole/quadrupole family modeling of paleosecular variation. *J. Geophys. Res.*, 93:11583–11588.
- McFadden, P.L., and Reid, A.B., 1982. Analysis of paleomagnetic inclination data. *Geophys. J. R. Astron. Soc.*, 69:307–319.
- McNutt, M.K., and Fischer, K.M., 1987. The South Pacific superswell. *In* Keating, B.H., Fryer, P., Batiza, R., and Boehlert, G.W. (Eds.), *Seamounts, Islands, and Atolls*. Geophys. Monogr., Am. Geophys. Union, 43:25–34.
- Merrill, R.T., and McElhinny, M.W., 1983. *The Earth's Magnetic Field: Its History, Origin, and Planetary Perspective*. London (Academic).
- Nakanishi, M., Gee, J.S., and Scientific Party ODP Leg 144, 1993. Paleomagnetic studies of the northwestern Pacific guyots (Part 2) [paper presented at 94th SGPSS Fall Meeting, Kobe, October 1993].
- Premoli Silva, I., Haggerty, J., Rack, F., et al., 1993. *Proc. ODP, Init. Reps.*, 144: College Station, TX (Ocean Drilling Program).
- Sager, W.W., Duncan, R.A., and Handschumacher, D.W., 1993. Paleomagnetism of the Japanese and Marcus-Wake seamounts, Western Pacific Ocean. *In* Pringle, M.S., Sager, W.W., Sliter, W.V., and Stein, S. (Eds.), *The Mesozoic Pacific: Geology, Tectonics, and Volcanism*. Geophys. Monogr., Am. Geophys. Union, 77:401–435.
- Stacey, F.D., and Banerjee, S.K., 1974. *The Physical Principles of Rock Magnetism*. Amsterdam (Elsevier).
- Van Fossen, M.C., and Kent, D.V., 1993. A palaeomagnetic study of 143 Ma kimberlite dikes in central New York State. *Geophys. J. Int.*, 113:175–185.
- Winterer, E.L., Natland, J.H., van Waasbergen, R.J., Duncan, R.A., McNutt, M.K., Wolfe, C.J., Premoli Silva, I., Sager, W.W., and Sliter, W.V., 1993. Cretaceous guyots in the Northwest Pacific: an overview of their geology and geophysics. *In* Pringle, M.S., Sager, W.W., Sliter, W.V., and Stein, S. (Eds.), *The Mesozoic Pacific: Geology, Tectonics, and Volcanism*. Geophys. Monogr., Am. Geophys. Union, 77:307–334.
- Zijderveld, J.D.A., 1967. AC demagnetization of rocks: analysis of results. *In* Collinson, D.W., Creer, K.M., and Runcorn, S.K. (Eds.), *Methods in Palaeomagnetism*. New York (Elsevier), 254–286.

* Abbreviations for names of organizations and publications in ODP reference lists follow the style given in *Chemical Abstracts Service Source Index* (published by American Chemical Society).

Date of initial receipt: 31 January 1994

Date of acceptance: 7 July 1994

Ms 144SR-022

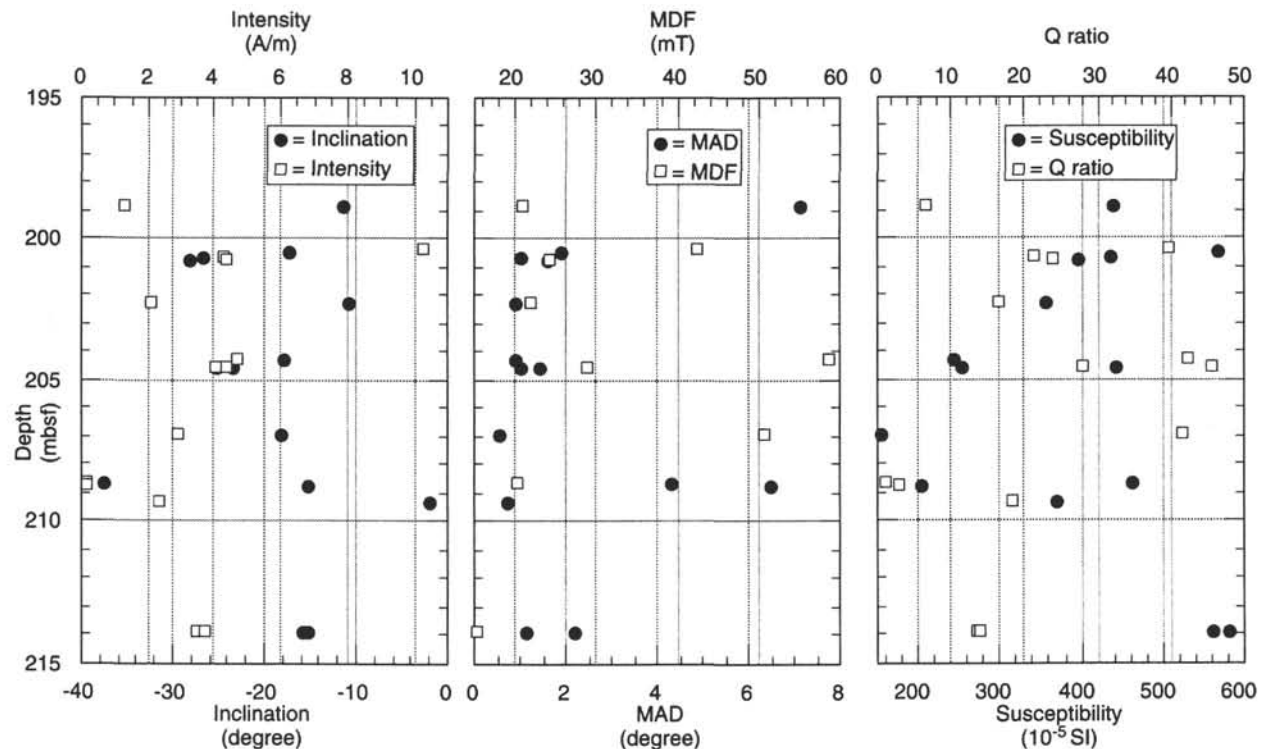


Figure 17. Paleomagnetic parameters, inclinations, NRM intensities, MADs, MDFs, susceptibilities, and Q ratios of the volcanic basement in Hole 878A vs. depth.

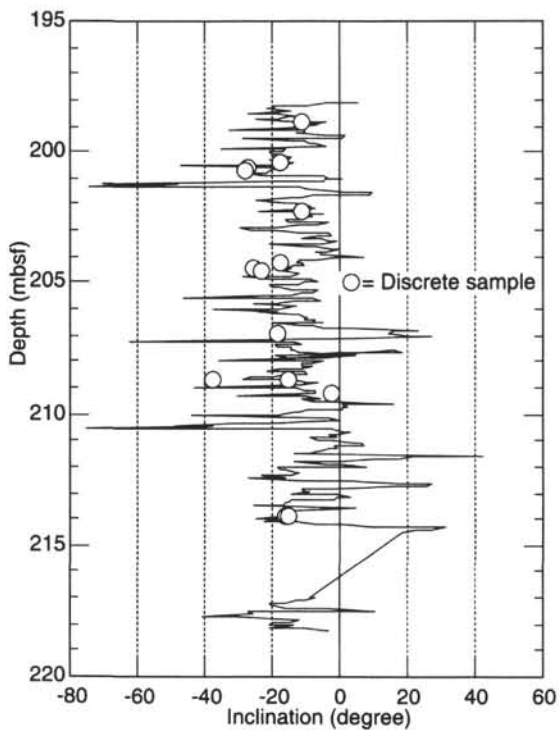


Figure 18. Result of the shipboard whole-core measurements of the volcanic basement from Takuyo-Daisan Guyot (Site 879) after AF demagnetization at 15 mT as well as those of discrete samples.

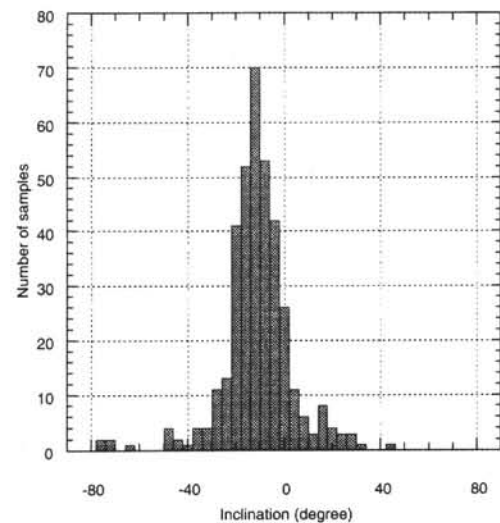


Figure 19. Histogram of inclinations of the volcanic basement from Takuyo-Daisan Guyot (Site 879) by whole-core measurements.

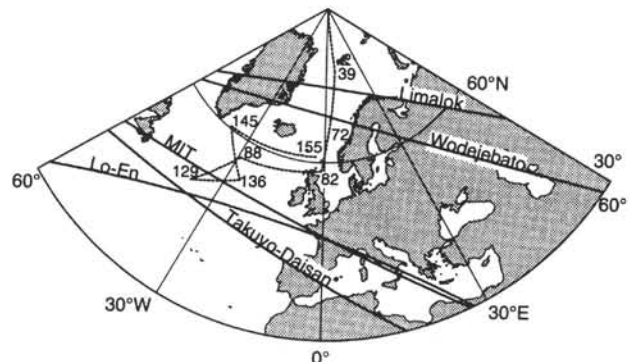


Figure 20. APWP of the Pacific Plate (Larson and Sager, 1992) with the locations of paleocolatitudes determined in this study. Dashed line = APWP, numbers near the dashed line = ages (Ma), and solid lines = paleocolatitudes.